Interaction between the Voltage-Dependent Sodium Channel and Calmodulin

Department of Physiological Sciences
School of Life Science
The Graduate University for Advanced Studies

Masayuki Mori

Contents

Abstract

The voltage-dependent sodium channel (VDSC) interacts with intracellular molecules to modulate channel properties and localizations in neuronal cells. To study protein interactions, I applied yeast two-hybrid screening to the cytoplasmic C-terminal domain of the main pore-forming α subunit. I found a novel interaction between the C-terminal domain and calmodulin (CaM). By two-hybrid interaction assays, I specified the interaction site of VDSC in a C-terminal region, which is composed of 38 amino acid residues and contains two calmodulin binding motifs, namely IQ-like and Baa motifs. Using a fusion protein of the C-terminal domain, I showed that interaction with CaM occurred in the presence and absence of Ca^{2+}. Two synthetic peptides, each covering the IQ-like (NaIQ) or the Baa motifs (NaBaa), were used to examine the binding property by a gel mobility shift assay. Although the NaIQ and NaBaa sequences are overlapped, NaBaa binds only to Ca^{2+}-bound calmodulin (Ca^{2+}CaM), whereas NaIQ binds to both Ca^{2+}CaM and Ca^{2+}-free calmodulin (apoCaM). Fluorescence spectroscopy of dansylated CaM showed Ca^{2+}-dependent spectral changes not only for NaBaa·CaM but also for NaIQ·CaM. These results indicate that whereas the NaBaa·CaM complex is formed in a Ca^{2+}-dependent manner, the NaIQ·CaM complex has two conformational states, distinct in respect to the peptide binding site and the CaM conformation, depending on the Ca^{2+} concentration. These observations suggest the possibility that VDSC is functionally modulated through the direct CaM interaction and the

Ca^{2+}-dependent conformational transition of the complex.

Abbreviations: aa, amino acid residues; CaM, calmodulin; CBS, CaM Binding Site; CD, circular dichroism; EDAC, 1-ethyl-3(3-dimethylaminopropyl)carbodiimide; EGTA, ethylene glycol bis(*β*-aminoethylether)-*N,N,N',N'*-tetraacetic acid; ESI-MS, electrospray-ionization mass spectrometry; Hepes, 2-[4-(2-hydroxyethyl)-1-piperazinyl] ethanesulfonic acid; PAGE, polyacrylamide gel electrophoresis; rBII, rat brain voltage-dependent sodium channel typeII; SD medium, minimal synthetic dropout medium; Tris, tris-(hydroxymethyl) aminomethane; VDSC, voltage-dependent sodium channel.

Introduction

The voltage-dependent sodium channel (VDSC) is essential to generating action potentials in many excitable cells. The α-subunit of VDSC is the main component of the channel responsible for voltage-sensitive gating and selective ion permeation (*1*). This α-subunit could conceivably be modulated through interaction with associated proteins to regulate action potential generation. In fact, the electrophysiological response of VDSC typeIIA, a splicing variant of VDSC typeII (*2*), is modulated by direct binding of G protein subunits, Gβγ, to the C-terminal domain of the channel protein (*3*). VDSC also interacts with the actin-associated proteins, ankyrin and spectrin (*4*), which regulate channel localization, and AKAP15, which regulates phospholylation (*5*). Most of the above findings for the proteins interacting with VDSC are based, however, on indirect or functional observations.

To establish a solid biochemical basis for analyzing intracellular events regulating VDSC, I looked for proteins that directly interact with VDSC intracellularly, using yeast two-hybrid screening system (*6*), focusing on the C-terminal domain of VDSC typeII. This domain is located intracellularly and exhibits greater sequence diversity among the various α-subunits than in other regions of the protein.

Through yeast two-hybrid screening, I identified a novel interaction of VDSC with calmodulin (CaM). CaM, a ubiquitous small (16.7 kDa) calcium-binding protein, acts as an intracellular Ca^{2+} sensor, which translates Ca^{2+} signals into cellular responses by interacting with target molecules (*7*). Previous studies on the *Paramecium* calcium-dependent sodium

channel showed that CaM binding to the channel itself or a channel-associated protein modulates activity of this type of sodium channel (*8*, *9*). In addition, recent observation has shown that the CaM interaction also modulates functions of other channels, such as the rod cGMP-gated cation channel (*10*, *11*), the *N*-methyl-D-aspartate (NMDA) receptor channel (*12*), the calcium-activated potassium channel (*13*), and the voltage-dependent calcium channels (VDCC) (*14*, *15*, *16*, and *17*). Whereas their common feature is their coupling to cytoplasmic Ca^{2+} regulation, VDSC is not known to directly couple to the Ca^{2+} signaling. In this work, I studied the novel interaction between CaM and VDSC, and the consequent Ca^{2+}-dependent structural transition of the CaM-VDSC complex. Binding of CaM with ion channels and receptors usually modulate those electrophysiological functions, for example, CaM mediates calcium-dependent inactivation of the voltage-dependent calcium channels. To test the hypothesis of functional alternations of VDSC by the direct CaM interaction, I performed electrophysiological analyses of VDSC.

Materials and Methods

Materials.

Hepes, dansyl chloride, and EGTA of the highest purity grade were obtained from Sigma Co. Dr. M. Noda (National Institute for Basic Biology, Japan) kindly provided the rat brain VDSC typeII cDNA, pRII-2A (*18*). Two synthetic peptides, NaIQ and NaBaa derived from the VDSC sequence (*2*), were obtained from Bio-Synthesis Inc. The peptides were purified by high-performance liquid chromatography and verified by mass spectrometry.

Methods.

Two-Hybrid Screening. Yeast two-hybrid screening was done using Matchmaker Two-Hybrid System 2 (Clontech). Bait was constructed in the plasmid pAS2-1C (provided by Dr. T. Maeda, University of Tokyo, Japan), which carries the cDNA sequence that encodes the Gal4 DNA binding domain. Plasmid pAS2-1C was constructed by replacing the 2 μm origin of pAS2-1 (Clontech) with the *CEN-ARS* origin (*19*). The efficiency of Y190 yeast cell transformation with pAS2-1C was 10 times higher than that with the original pAS2-1. The VDSC cDNA fragment encoding the C-terminal domain of the rat brain VDSC typeII was amplified by PCR using HF DNA polymerase (Boehringer Mannheim) with the following primers:

Sense primer: 5'-CGCCATATGGAGAATTCACGTCGCC-3'

Antisense primer: 5'-CGCCTGCAGTTACTTTTTACTTTCCCTGAT-3',

with pR2-IIA as a template. The amplified cDNA fragment (encoding amino acid residues 1777–2005; see Ref. *2*) was inserted into the *Nde*I–*Pst*I site of pAS2-1C to yield bait plasmid pBDVDSCC1. The nucleotide sequence of the bait construct was confirmed by ABI 377 DNA sequencer (Perkin-Elmer Co.). The two-hybrid screening and the interaction assay were performed essentially as described in the Matchmaker 2 protocol (Clontech). Strain Y190 yeast cells containing *LacZ* and *His3* reporter genes with upstream *Gal4* operators were transformed with bait plasmid pBDVDSCC1. Y190 cells containing the bait plasmid were retransformed with a rat brain cDNA library (Clontech) by a lithium acetate method. Transformants were plated on minimal medium lacking leucine, tryptophan, and histidine in the presence of 25 mM 3-amino-1,2,4-triazole (SD/–Leu/–Trp/–His/+3-AT) and incubated for 7 days at 30°C. This yielded 5.5×10^6 Leu^+ and Trp^+ transformants (2×10^5/μg DNA). Two-hybrid screening system is summarized in Figure 1. β-Galactosidase assay of His^+ cells was conducted as described in the Matchmaker 2 protocol.

Two-hybrid Interaction Assay of the VDSC C-terminal Domain with CaM. The cDNA fragment encoding the VDSC C-terminal domain was mutated by PCR to obtain deleted or truncated mutants. These cDNA fragments were introduced into pAS2-1C to yield mutant bait plasmids pBDVDSCC2 (encoding amino acid residues 1777–1938), pBD4VDSCC3

(1777–1900), pBDVDSCC4 (1866–2005), and pBDVDSCC5 (1777–1900 and 1939-2005) (Figure 2). The nucleotide sequences of the bait constructs were confirmed by the dye terminator method. One of the mutant bait plasmids and the plasmid encoding rat CaM (pADCaM), identified through the yeast two-hybrid screening, were cotransfected into Y190 cells. Transformants were plated onto SD/–Leu/–Trp/–His/+3-AT plates and incubated for 5 days at 30°C. Reporter gene *LacZ* activity was studied using β-galactosidase assay as described in the Matchmaker 2 protocol.

Fusion Proteins. Expression plasmids for two S-Tag proteins were constructed in pET32a (Novagen). Plasmid pETS-tagC-term contained the cDNA sequence encoding the entire C-terminal domain (amino acid residues 1777–2005). Plasmid pETΔCBS, which contains the cDNA encoding amino acid residues 1777–1900 and 1939–2005 (missing Region 2), was constructed by PCR using the following oligonucleotide primers: 5'-CGC CTC GAG TTA CAG GGT GGT GGT AAT-3' and 5'-GAC AAA GGT AAA GAA GAC GAG GGA-3'. Plasmid pETC-termEQ was constructed by mutating the cDNA so that the isoleucine residue (1912) in the IQ-motif was replaced by a glutamic acid residue; the primers used were 5'-GCT ATT GTC GAA CAG CGA GCA-3' and 5'-GCT CGT TGT TCG ACA ATA GCA GA-3'. Furthermore, plasmid pETC-termE4 was constructed by mutating the cDNA so that the amino acid residues KVKK (1924-1927) in the IQ-motif are conversed to EEEE; the primers used

were 5'-GAA GCA GAA AGA GGA GGA GGA GTC GTC TAT C-3' and 5'-AGA CGA CTC CTC CTC CTC TTT CTG CTT CAG G-3'. Mutations were introduced into C-terminal domain of VDSC cDNA by PCR reactions. The mutations were confirmed by the nucleotide sequencing.

Bacterial cells of *E.coli* BL21(DE3)pLysS (*20*) were transformed by each plasmid, and two fusion proteins were expressed as described in the protocol (Novagen). To purify fusion proteins, bacterial lysates were applied to nickel-Sepharose columns. Eluted fractions were checked for purity by Coomassie Brilliant Blue staining of SDS-PAGE. Purified fusion proteins were digested with thrombin to remove the thioredoxin and His-tag region.

Pull-Down Assay. Mixtures of rat brain extracts [100 μg of protein in total volume (1 mL)], S-tag protein (10 μg of protein in total volume), and S-protein agarose (Novagen; 50 μL) that specifically binds to S-tag proteins (*21*) were incubated for 30 min at 4°C in the following solutions: 50 mM Hepes/Tris (pH 7.3), 150 mM KCl, and 1% Nonidet P-40 in the presence (0.5 mM Ca^{2+}) or absence (2 mM EGTA) of Ca^{2+}. Mixtures were then washed 5 times with buffer (1 mL × 5). After brief centrifugation, proteins bound to the agarose were eluted with SDS-PAGE sample buffer (50 μL), and 15 μL of each sample was applied to a 12.5% gel. After electrophoresis,the gel was electroblotted onto a nitrocellulose membrane (Bio-Rad). CaM was detected by an anti-CaM monoclonal antibody (Upstate

Biotechnology) and alkaline phosphatase-linked secondary antibody (Bio-Rad), and visualized by chemiluminescence (NEN).

Chemical Cross-Linking. Ten nano moles S-tag protein (S-tagC-term and S-tagC-termΔCBS) with fourty nmoles of CaM were incubated in 200 μL of 50 mM Mes-HCl pH 7.0 at room temperature for ten minutes and then treated with 750 μM of 1-ethyl-3(3-dimethylaminopropyl)carbodiimide (EDAC) for two hours, and S-tag protein alone as a control. The reaction was stopped by acidification with 1% trifluoroacetic acid. After lyophilyzation, the cross-linked proteins were dissolved in SDS-PAGE sample buffer (100 μL), and 20 μL of each sample was applied to a 12.5% gel. After electrophoresis, gel was electroblotted onto a nitrocellulose membrane. S-tag proteins were detected by an alkaline-phospatase labelled S-protein (Novagen), and visualized by chemiluminescence (NEN).

Gel mobility shift assay. Different concentrations of peptides derived from VDSC (NaIQ and NaBaa) were incubated with 2 μM CaM (purified as ref. 22), in 30 mM Hepes/Tris pH 7.3, 150 mM KCl, 0.1% Nonidet P-40, and 1 mM $CaCl_2$ or 2 mM EGTA for 30 min at room temperature. These mixtures were loaded on nondenaturing 12.5% polyacrylamide gels containing 1 mM $CaCl_2$ or 2mM EGTA and visualized by silver staining.

Dansylation of CaM. Dansylated CaM (dansyl-CaM) was prepared using rat brain CaM and dansyl chloride as described previously (*23*). Additionally, the dialyzed mixture of dansyl chloride with CaM was applied to a PD-10 column (Sephadex-25G, Pharmacia) to remove remaining free dansyl chloride.

Fluorescence Spectroscopy. Fluorescence spectra were recorded in a quartz cuvette (light path: 10 mm), using a Hitachi F-4500 fluorescent photometer. Each peptide dissolved in distilled water was added to a cuvette containing dansyl-CaM. The concentration of dansyl-CaM was 120 nM in 30 mM Hepes/Tris (pH 7.3), 150 mM KCl, and 1 mM $CaCl_2$ or 2 mM EGTA. To ensure equilibration of the mixture, the sample was constantly stirred for 15 min at 25 ℃ before measurement. The excitation wavelength (Ex) was 340 nm, the measured emission wavelengths (Em) was 400 - 600 nm, and both of excitation and emission band widths were 10 nm. The fluorescence spectrum for each sample is an average of five scans. For the titration experiments, the fluorescence intensity was measured at Em 480 nm integrated for 5 seconds for each sample. The binding model used to fit the dansyl fluorescence data was simply

$$\text{pep} + \text{CaM} \leftrightarrow \text{pep} \cdot \text{CaM}$$

where pep is the peptide (NaBaa or NaIQ) and $\text{pep} \cdot \text{CaM}$ the peptide-CaM complex. The dissociation constant K_d is

$$K_d = \frac{([CaM]_0 - [pep \cdot CaM])([pep]_0 - [pep \cdot CaM])}{[pep \cdot CaM]} \qquad (1)$$

where $[CaM]_0$ is the initial concentration of CaM and $[pep]_0$ that of the peptide.

Fluorescence intensity is assumed to be a linear function of $[pep \bullet CaM]$,

$$F_{480} = F_b [pep \cdot CaM] + F_0 \qquad (2)$$

Experimental fluorescence data given as a function of $[pep]_0$ was fitted by combining of Eq. (1) and (2) using a nonlinear least-squares program (Levenberg-Marquardt algorithm) (*25*) run on a personal computer. Fitting parameters were F_b, F_0 and K_d.

Ca^{2+}-dependence of Fluorescence. Fluorescence intensity was obtained at Em 480 in 30 mM Hepes/Tris pH7.3, 150 mM KCl, and 2 mM EGTA, containing 120 nM dansyl-CaM, and 250 nM NaIQ or 800 nM NaBaa, with an increasing concentration of Ca^{2+}. Relative fluorescence was calculated by the following equation:

Relative Fluorescence = $(F - F_0)/(F_{max} - F_0)$,

where F is the measured intensity, F_{max} is the maximum intensity, and F_0 is the intensity without added Ca^{2+}.

Identification of Dansylated Site in Dansyl-CaM. The molecular weights of CaM and dansyl-CaM were determined by an electrospray-ionization mass spectrometer ESI-MS API-300 (Perkin-Elmer), to calculate the number of dansylated sites in a dansyl-CaM molecule.

To identify the specific dansylation site, CaM and dansyl-CaM (50 μg of each) were digested by trypsin (Sigma) in 20 mM Tris/pH 8.0 with HCl, 100 mM NaCl, 1mM $CaCl_2$, 2 M urea, and 1% of CaM or dansyl-CaM for 4 h at room temperature. Tryptic peptides were separated out using a SMART system with a μRPC C2/C18 column (Pharmacia). The mobile phase was 0.1% trifluoroacetic acid and an increasing gradient of 0-50% acetonitrile for 50 min at room temperature. Separated fractions were lyophilized and dissolved in distilled water (total volume of 200 μl). A fluorescence micro-plate reader MTP-100F (Corona Electric) was used to measure the fluorescence of the lyophilized fractions with Ex 360 nm and Em 500 nm. Only one specific fraction of the dansyl-CaM products showed strong fluorescence emission, and the amino acid sequence of the fraction was determined by the Edman method. Automated sequence analysis was conducted using an ABI494 protein sequencer (Applied Biosystem), and phenylthiohydantoin derivatives of amino acids were identified by reverse-phase high-performance liquid chromatography.

Circular Dichroism. Circular dichroism (CD) spectra were measured with a J-720WI spectropolarimeter (Jasco) using a quartz cuvette with a light path of 2 mm at 25°C in 30 mM Hepes/Tris (pH 7.3), 150 mM KCl, and 0.5 mM $CaCl_2$ or 5 mM EGTA. Spectra were obtained by scanning at 100 nm/min over a wavelength range of 190–250 nm. Far-UV CD spectra were measured at 10 μM peptide and 5 μM CaM. For each sample, 16 scans were

averaged. Means residue of molar ellipticity [θ] was determined from the relationship: [θ]= (θ / 10·c·d·r), where θ is the ellipticity in degrees, c the protein concentration (M), d the path length (cm), and r the number of amino acid residues (148 in the case of CaM). The ellipticity of the mixture was obtained by subtracting the record of the peptide alone measured in advance.

CaM-agarose Binding Assay. CaM-agarose (Sigma) was washed four times with 50 mM Hepes/pH 7.3 with Tris, 150 mM KCl, and 1% Nonidet P-40. 10 μg of purified S-tag proteins [S-tagC-term (full C-terminal), S-tagC-termΔCBS (CBS-deletion mutant), S-tagC-termEQ (I1912E mutant), and S-tagC-termE4 (KKVK-to-EEEE mutant)] in 200 μL of the same buffer were mixed with CaM-agarose (50 μL) in the presence (0.5 mM Ca^{2+}) or absence (2 mM EGTA) of Ca^{2+} at room temperature for 30 min under gentle agitation. After washing by brief centrifugation, the pellets were solubilized with 50 μL of a SDS-PAGE sample buffer. S-tag proteins were detected by alkaline phosphatase-conjugated S-protein (Novagen).

Functional Expression of VDSC. In this study wild-type (WT) and mutant VDSC cDNAs were inserted in the mammalian expression vector pCI-neo (Promega). The cDNA encoding the rat brain typeII (rBII) sodium channel α–subunit in pRII-2A (18) was digested with *Eco*RI / *Apa*I and *Apa*I / *Sal*I. The resultant fragments were ligated with the *Eco*RI / *Sal*I vector

fragment of pCI-neo to yield pCI-neo-rBII-WT. A mutant which lacks the CaM binding site in rBII (pCI-neo-rBIIΔCBS) could not be functionally expressed in HEK 293 cells. Another mutant in which a stretch of amino acid sequence KKVK (1924-1927a.a. in rBII) was changed to EEEE was constructed in pCI-neo vector (pCI-rBIIE4). This mutant could be functionally expressed. This mutant should function as a loss-of-function mutant for the apoCaM interaction. Therefore, in the present study, the research target for the function of rBII is apoCaM interaction.

Either pCI-neo-rBIIWT or pCI-neo-rBIIE4 was cotransfected with a plasmid which carries the cDNA encoding the T-cell antigen CD8 (Jurdman et al., 1994) into HEK 293 cells by using LipofectAMINE Reagent (Gibco BRL). Cells were grown to 75 % confluence in 35 mm tissue culture dishes and transfected with 1 μg of plasmids for the Na^+ channel α-subunit and CD8 in a mass ratio of ~1:0.5. After addition of the plasmids, cells were maintained in Dulbecco's modified Eagle's medium (DMEM) at 37°C in 5% CO_2. 12 h after transfection, the cells were removed from the dishes using trypsin-EDTA solution (Gibco BRL), and replated on glass plates at low density for electrophysiological recordings. Positive transfectants were identified by their binding of anti-CD8-coated beads (Dynabeads M-450 CD8; Dynal, Great Neck, NY).

Electrophysiological Recordings. I conducted whole-cell patch-clamp recordings at room temperature using an EPC-9 amplifier (HEKA Electronic, Lambrecht, Germany). Data were

acquired on a PC computer with the Pulse program (v. 7.52, HEKA Electronic). Patch pipette were made from aluminosilicate glass capillaries (1.6 mm outer diameter, Hilgenberg, Malsfeld, Germany) using a model P-87 Flaming-Brown micropipette puller (Sutter Instrument, San Rafael, CA). Pipette resistance ranged from 1 to 3 MΩ when filled with the pipette solution described below. Voltage-clamp errors were minimized by 80 % series resistance compensation, and the capacitance artifact was canceled by the computer-controlled circuitry of the patch-clamp amplifier and by a P/6 method. Membrane currents were filtered at 10 kHz and sampled at 50 kHz. The pipette solution contained 70 mM CsF, 60 mM CsCl, 12 mM NaCl, 10 mM HEPES, 0.5 mM EGTA (pH 7.4 with CsOH). The bathing solution was 135 mM NaCl, 10 mM HEPES, 10 mM glucose, 1.5 mM $CaCl_2$ and 1.5 mM $MgCl_2$ (pH 7.4 with NaOH). The osmolarity of both solutions was adjusted to ~295 mOsm (VOGEL OM801 osmometer).

Data Analysis of the Electrophysiological Experiment. Data analysis was performed on a PC computer, using the Pulse fit (v. 8.31, HEKA) and IgorPro (WaveMetrics, Lake Oswego, OR). The parameters for voltage dependence of activation were estimated from the current-voltage relation based on the equation, $I=G_{max}*(V-V_{rev})/(1+\exp(-(V-V_m)/k_m))$, where I is the peak current amplitude, G_{max} the maxmum conductance, V test potential, V_{rev} the reversal potential, V_m the midpoint of activation, and k_m a slope factor. If one assumes that the

process of inactivation involves only two states, variation of the steady-state probability with potential should follow a Bolzmann distribution. Therefore, voltage-dependence of inactivation curves were fitted to the Boltzmann function

$$\frac{I}{I_{peak}} = \frac{1}{1 + \exp\left(\frac{V - V_h}{k_h}\right)}$$

where I_{peak} is the maximum peak current measured, V_h is the midpoint of the curve, and k_h is the slope factor.

The time constant for the recovery from the inactivated state was obtained by fitting the relationship between peak amplitude and interpulse duration using a double pulse protocol (Figure 16). The relationship was fitted by a single exponential function $[1-\exp(-t/\tau_h)]$, where τ_h is the time constant for recovery. All data reported in this study are expressed as standard error of the mean (S.E.M).

Results

Two-Hybrid Screening. To search for proteins that interact with the C-terminal domain of VDSC typeII (*2*), I used the yeast two-hybrid screening of an expression cDNA library from rat brain with 5.5×10^6 independent clones, and obtained 20 positive colonies. Four of the positive clones carried full-length rat calmodulin (CaM) cDNA (*27*) (plasmid: pADCaM). Remainders of the positive clones were found to encode only short peptides (10 to 15 amino acid residues) fused with the Gal4 DNA activation domain, and were not studied further.

Two-Hybrid Interaction Assay. Reports on CaM-binding proteins have shown that CaM binds to several consensus sequence motifs, such as the Baa motif (basic amphipathic α-helix) (*28*) and the IQ motif (IQXXXRGXXXR; where X is any amino acid) (*29*, *30*). I searched for these types of CaM binding motifs in the VDSC C-terminal domain to find two candidate regions for CaM binding (designated Region 1 and Region 2; Figure 2A). Region 1 (amino acid residues 1852–1866) has a Baa motif, whereas Region 2 (1919–1933) has both Baa and IQ-like motifs.

To determine whether Region 1 and Region 2 are actual CaM binding regions, I performed a two-hybrid interaction assay using four mutated C-terminal domains of the VDSC α-subunit as bait proteins (Figure 2A and Figure 3). Y190 cells were cotransfected with pADCaM and one of the bait plasmids. Y190 cells cotransfected with pADCaM and pBDVDSCC5

(containing Region 1 but not Region 2) did not grow on selection plates. Cells cotransfected with pADCaM and pBDVDSCC3 (containing Region 1 but not Region 2 and the following residues) grew feebly on selection plates, but β-galactosidase activity was not detected. In contrast, cells cotransfected with pADCaM and one of the pBDVDSCC1, 2, or 4 (all containing Region 2) showed moderate or high β-galactosidase activity. The results of the two-hybrid interaction assay indicate that Region 2 is a CBS (CaM binding site) in the VDSC C-terminal domain in the yeast two-hybrid system. This result is summarized in Figure 2A.

Pull-Down Assay. Ca^{2+}-dependence of CaM binding to its target proteins is the critical property that controls the binding process. However, in the yeast two-hybrid system, it is difficult to determine whether the CaM molecule is Ca^{2+}-free apoCaM or Ca^{2+}-bound Ca^{2+}CaM because this system detects molecular interaction in an intranuclear environment (*6*). I studied the Ca^{2+} dependence of binding between Region 2 and CaM using a pull-down assay. Two S-tag proteins, one carrying the full-length C-terminal protein (S-tagC-term) and the other having the C-terminal domain without CBS (S-tagC-termΔCBS), were bound to S-protein agarose, and purified CaM was adsorbed to the S-tag protein-agarose complex. Immunoblot analysis using an anti-CaM antibody showed that CaM was detected only in the mixture of CaM and the agarose containing S-tagC-term, either in the presence or in the absence of Ca^{2+}, but not in mixtures containing S-tagC-termΔCBS or the control S-protein

(Figure 4). Binding of CaM with S-tagC-term was even stronger in the absence of Ca^2 than in the presence of Ca^{2+}.

Chemical Cross-Linking. To determined the CaM binding ratio in the C-terminal domain of VDSC, I used a cross-linker EDAC [1-ethyl-3(3-dimethylaminopropyl)carbodiimide]. This water-soluble reagent crosslinks a specific amine and carboxylic acid between proteins in the complex (*31*). Because ionic interactions are known to play a prominent role in forming complex between CaM and target molecules (*32*), the acidic residues present in the CaM structure were selected for cross-linking formation. Following the complex of CaM with S-tag protein interaction, carboxyl groups were activated by EDAC and allowed to react with amino groups to form covalent inter-molecular bonds. Finally, the molecular weight of the complex was determined by SDS-PAGE. Even in the presence or in the absence of Ca^{2+}, the S-tagC-term protein was ~52kDa (S-tagC-term, in Figure 5), and the complex with CaM was ~70 kDa (S-tagC-term/CaM in Figure 5). Because the molecular weight of CaM is known to be ~17 kDa (*7*), the result indicates that CaM interacts at the stoichiometrical ratio of 1:1 with the C-terminal domain in the presence or absence of Ca^{2+}.

Gel Mobility Shift Assay. Region 2 contains both IQ-like and Baa motifs. I prepared two synthetic peptides, "NaIQ" and "NaBaa", whose sequences contain the IQ-like and the

Baa motif, respectively (the amino acid sequences are described in figure 2B). I then analyzed the binding properties between peptides and CaM in a gel mobility shift assay. In the presence of Ca^{2+}, CaM preincubation with either NaIQ or NaBaa delayed the mobility of the CaM band (Figures 6A and C). Mixtures of higher ratios of either peptide to CaM showed a larger population of the slowly mobile CaM band. A complete shift of the mobility occurred at the peptide to CaM ratio of 4:1 for NaIQ (Figure 6A), while NaBaa caused no complete shift under our experimental conditions (Figure 6C). Thus, in the presence of Ca^{2+}, CaM was able to bind to both peptides with a higher affinity for NaIQ than for NaBaa (compare Figure 6A and Figure 6C). In the absence of Ca^{2+} (2 mM EGTA), no band shift was observed for the mixture of NaBaa and CaM (Figure 6D), whereas the NaIQ and CaM mixture still strongly delayed CaM band mobility (Figure 6B). A complete shift occurred at an NaIQ-CaM molar ratio of 2:1. The results demonstrated that whereas the interaction between the Baa motif and CaM is Ca^{2+}-dependent, the IQ-like motif of VDSC can bind to CaM in a Ca^{2+}-independent manner.

Fluorescence Spectroscopy. Binding of the two peptides with CaM was also studied using dansylated CaM (dansyl-CaM). Dansyl-CaM is a useful tool to detect interactions between CaM and other proteins and conformational changes of CaM, because the fluorescence spectrum is shifted and the intensity is enhanced when the environment of the

dansyl moiety becomes hydrophobic (*33*). In the presence of Ca^{2+}, the blue shift and enhancement of the dansyl fluorescence spectrum were observed when 300 nM of NaIQ peptide or NaBaa peptide was added (Figure 8). To quantitative binding analysis, I applied peptide titration. Apparent dissociation constants (K_d) obtained by fitting experimental results using a nonlinear least-squares program were 4.6 nM for NaIQ·dansyl-Ca^{2+}CaM and 89.7 nM for NaBaa·dansyl-Ca^{2+}CaM (Table 2), suggesting that Region 2 of VDSC contains two CaM binding sites with different affinities to CaM.

In the absence of Ca^{2+}, as suggested that from the result of the gel mobility shift assay, NaBaa did not alter the fluorescence spectrum, confirming that NaBaa does not bind to dansyl-CaM (Figure 7B). Surprisingly, addition of 300 nM of NaIQ failed to affect the fluorescence spectrum (Figure 7A), although the results of the gel mobility shift assay described above unambiguously indicated that NaIQ binds to apoCaM (Figure 6B). To solve this apparent discrepancy, I conducted a series of experiments. At first, I tested the effect of dansylation on the gel mobility shift assay. Using dansyl-CaM instead of CaM, NaIQ equally shifted the CaM band in the absence of Ca^{2+} (Figure 9). This result indicates that NaIQ can bind to dansyl-CaM Ca^{2+}-independently to form the NaIQ·dansyl-apoCaM complex, excluding the possibility that addition of the dansyl moiety prevents NaIQ from binding to CaM. Second, I determined the number of dansylated sites in a dansyl-CaM molecule using ESI-MS. The measured molecular weight of CaM is 16791.33 (predict

16790.52), and the dansyl-CaM is17024.24. The difference of molecular weight between the CaM and the dansyl-CaM correspond to a dansyl moiety (M.W. 233.1). Third, I then identified Lys_{75} as the dansylated site by determining the amino acid sequence of the fluorescent tryptic peptide (Figure 10), consistent with the previous report (*34*). Lys_{75} is located near the flexible linker (amino acid residues 77-80), which connects the N- and C-terminal globular Ca^{2+} binding domains of CaM (*35, 36*). Taken together, although NaIQ and dansyl-CaM bind in the presence and absence of Ca^{2+}, the binding in the presence of Ca^{2+} alters the fluorescence spectrum, whereas the binding in the absence of Ca^{2+} cannot be detected by spectroscopy, indicating that the NaIQ-CaM complex has two different conformational states, interchanging Ca^{2+} dependently.

To analyze of the Ca^{2+} dependency of the conformational states, I applied Ca^{2+} titration (Figure 11). Without peptides, dansyl-CaM exhibited fluorescence changes in a Ca^{2+} concentration range of 0.5 to 2 μM. The fluorescence changes of the NaBaa·dansyl-CaM complex occurred in a much lower Ca^{2+} concentration range, which may correspond to a physiological Ca^{2+} concentration. The NaIQ·dansyl-CaM complex showed an intermediate Ca^{2+} dependency.

CD Spectroscopy. Protein-protein interaction can be detected by the conformational analysis of proteins. Far-UV CD spectroscopy is a powerful tool for detecting changes in the

secondary structure of CaM induced by binding with peptides (*37*). The CD spectral measurements were performed here to detect conformational changes accompanied by the formation of the NaIQ·CaM complexes. The bee venom peptide melittin (peptide of 26 amino acid residues; **GIGAVLKVLTTGLPALISWIKRKRQQ**) was used as a control. Melittin binds to CaM with a very high affinity in a Ca^{2+}-dependent manner (*36*, *37*).

In the presence of Ca^{2+}, the spectrum of the NaIQ-Ca^{2+}CaM mixture showed enhanced negative ellipticity compared to the spectrum of Ca^{2+}CaM alone (Figure 12A). This result indicated that the NaIQ·Ca^{2+}CaM complex shows a significant increase in α-helical content upon complex formation. In the absence of Ca^{2+}, the melittin-apoCaM mixture showed a marginal increase in α-helical content, as expected from little binding of melittin to CaM in the Ca^{2+}-free condition (Figure 12B). In contrast, the NaIQ-apoCaM mixture showed significantly enhanced negative ellipticity at around 222 nm, indicating that NaIQ binds to apoCaM even in the absence of Ca^{2+}, and that the α-helical structure was induced upon formation of the NaIQ·apoCaM complex. Furthermore, the spectra of the NaIQ·Ca^{2+}CaM and NaIQ·apoCaM complexes were slightly but significantly different (Figure 12B, inset). Because the helical change in CaM conformation induced by Ca^{2+} (without peptide) has been reported to correspond to about 11 amino acid residues (*40*, *41*), a simple estimate suggests that the spectral amplitude change from NaIQ·apoCaM to NaIQ·Ca^{2+}CaM (ca. 40% of without peptide) corresponds to the formation of α-helix of four to five residues. The α-helix

inducible site of CaM is speculated under Discussion.

Electrophysiology of CaM binding effect for the Sodium Channel. Because the CBS-deletion mutant of rBII (rBIIΔCBS) could not be functionally expressed in HEK 293 cells, another site-directed mutant (E4), in which the KKVK sequence in CBS (1924-1927a.a. in rBII) was chnaged to EEEE, was constructed in pCI-neo vector (pCI-rBIIE4). This mutant channel should function as a loss-of-function mutant for apoCaM binding on the basis of the observation in the CaM-agarose binding assay (Figure 13). Interestingly, mutating Ile 1912 to Glu (S-tagC-termEQ) did not significant affect the CaM binding in the presence or absence Ca^{2+}, although the Ile residue of the IQ-motif in the L-type VDCC is reported to play an important role in interacting with Ca^{2+}CaM (*16*).

Patch-clamp studies on HEK293 cells expressing recombinant rBIIWT demonstrated a tetrodotoxin (TTX)-sensitive sodium current. The WT and E4 channels have similar *K*i values for TTX, 4.5±0.31 nM (n=3) for WT and 5.1±0.45 for E4 (n=3). Non-transfected HEK293 cells have some endogenous sodium current of at most 400 pA / cell, which is small enough, compared to the exogenously expressed currents. Figure 14B shows typical traces of the WT Na^+ current in response to depolarizing steps (Figure 14A). Figure 14C shows the peak current amplitude-voltage relationship of the WT and the E4 mutant. The bell-shaped curve has a peak at -11.6 ± 0.85 mV for WT (n=4) and -12.8 ± 1.2 mV for E4 (n = 4). The

voltage-dependence of inactivation was obtained using a conventional two-pulse protocol, illustrated in Figure 15A. The peak current evoked by the test pulse is expected to be proportional to the fraction of channels remaining in the resting (i.e., non-inactivated) state at the end of the prepulse. Figure 15C is the plot of I/I_{peak} against the prepulse potential. The midpoint of inactivation V_h was –70.6 mV with the slope factor k_h of 6.56 mV for WT (n=5), and –69.7 mV with 8.67 mV for E4 (n=4). The time course of recovery from inactivation was studied as described in the legend to Figure 16A. Fractional ratio represents the fraction of channels, which recovered from inactivation relative to its steady-state value (Figure 16B). Fitting with a single exponential function gave a satisfactory result. The time constant for recovery was 3.98 ms for WT and 4.05 ms for E4 (n=4 for both). Finally, I examined the effect of the divalent cations (barium and calcium) on Na+ channels. Barium used as a control for divalent cations, and the CaM's affinity for barium is very low. Fractional ratios (calcium / barium) was obtained by the peak amplitude at same divalent ions (1.5 mM, 5 mM, 10 mM). I found no significant difference between WT and E4 mutant, suggesting that the biochemical results were independent of the electrophysiological methods I used.

Discussion

Complex Formation of CaM and VDSC. I have discovered that the Ca^{2+}-binding protein CaM directly binds to the α-subunit of VDSC. CaM is known to bind to a wide range of functional proteins (*7*), and several consensus motifs for CaM binding have been proposed. I found two regions which contains the consensus motifs in the C-terminal domain of VDSC. The yeast two-hybrid interaction assay confirmed one of the two regions as an actual CaM binding site. The identified region, Region 2 (1901-1938 a.a. in rBII), contains the sequences of both Baa and IQ-like motifs for CaM binding. The Baa motif (basic amphipathic α-helix) of 15 to 20 residues has been found in several CaM-binding proteins and peptides, such as melittin (*38*, *39*), CaMKII (*42*), and MLCK (*43*). They bind to CaM Ca^{2+}-dependently. The IQ motif (IQXXXRGXXXR) of 11 residues is another CaM binding motif, found in proteins such as growth cone associated protein 43kDa (GAP-43/neuromodulin) (*44*, *45*), CNG channel β-subunit (*10,11*), and L-type VDCC (*17*, *18*) (Table 2). IQ motif proteins have more diverse Ca^{2+} sensitivity than Baa motif proteins. Some IQ motif proteins such as neuromodulin or neurogranin bind CaM preferentially in the absence of Ca^{2+} (*42*, *43*, *44*), some proteins only in the presence of Ca^{2+} (*17* and *18*), and other proteins Ca^{2+}-independently (*45*). In this work, I showed that the VDSC C-terminal domain binds to not only Ca^{2+}-bound Ca^{2+}CaM but also to Ca^{2+}-free apoCaM. CaM is well-known to be one of the primary Ca^{2+} sensors, regulating the activity of many target proteins when Ca^{2+}

binds to CaM (*7*). Nevertheless, the physiological significance of the Ca^{2+}-independent binding or the relationship between the Ca^{2+}-dependent and Ca^{2+}-independent binding has not been studied well. In the present case, Region 2 in the VDSC C-terminal domain presents such an interesting model of CaM binding, in which both Ca^{2+}-dependent and Ca^{2+}-independent interactions are involved.

Binding Site and Structure of NaIQ·CaM in the Presence and Absence of Ca^{2+}. I examined the CaM binding properties using two synthetic peptides NaIQ and NaBaa. Table 1 summarizes the results from three different series of experiments. While half of the residues (15 aa) of the NaIQ and NaBaa sequences are overlapped, the two peptides exhibit distinct Ca^{2+} dependency of CaM binding; NaBaa binds to CaM Ca^{2+}-dependently, and NaIQ binds to CaM Ca^{2+}-independently. Thus, the NaBaa sequence is sufficient for Ca^{2+}CaM binding but not for apoCaM binding, whereas the NaIQ sequence is essential for apoCaM binding. This observation suggests that the apoCaM and the Ca^{2+}CaM binding site on CBS are not identical.

Although NaIQ binds to CaM in a Ca^{2+}-independent manner, the fluorescence spectrum of NaIQ−dansyl-CaM mixture was found to depend on the Ca^{2+} concentration in the solution. Together with several supplementary experiments, I concluded that the conformation of the NaIQ-CaM complex is different depending on a Ca^{2+} concentration (see Results). Without

peptides, the state transition from apoCaM alone to Ca^{2+}CaM alone on addition of Ca^{2+} alters the fluorescence spectrum of dansyl-CaM (Figure 7). This change is caused by an α-helix formation of the flexible linker domain (consisting of 4 residues) in the close vicinity of which Lys_{75} resides (*41*). In the presence of Ca^{2+}, addition of NaIQ results in a more pronounced blue shift and a greater enhancement of the fluorescence, indicating that NaIQ binding greatly alters the environment in the vicinity of dansylated Lys_{75}. Direct contact of the peptide to Lys_{75} and more global conformational changes of CaM induced by peptide binding would cause those fluorescence changes (*46*). In the absence of Ca^{2+}, however, the fluorescence spectrum of NaIQ-apoCaM was practically identical to that of apoCaM, suggesting that NaIQ binds to apoCaM at a site away from Lys_{75}, and that the CaM flexible linker conformation was not affected on NaIQ binding. The notion that NaIQ binds to CaM at different sites Ca^{2+}-dependently is supported by the nuclear magnetic resonance study on the interaction between the IQ motif peptide "Neurop" derived from neuromodulin and apoCaM (*47*). This report show that the Neurop peptide binds to the C-terminal domain of CaM, but not to the flexible linker domain. As for the conformational difference of the peptide·CaM complex, our results of CD spectroscopy that a stretch of four to five residues forms an α-helix in the state transition from NaIQ·apoCaM to NaIQ·Ca^{2+}CaM, further supporting that CaM is in different conformational states depending on Ca^{2+}. Thus, NaIQ·apoCaM and NaIQ·Ca^{2+}CaM are in two conformational states, distinct with respect to

the peptide binding site and the CaM conformation.

The Ca^{2+} titration experiments in Figure 11 for CaM alone, NaBaa-CaM and NaIQ-CaM provide information about the conformational transitions;

$$CaM + nCa^{2+} \rightarrow CaM \cdot nCa^{2+}$$
$$NaBaa + CaM + nCa^{2+} \rightarrow NaBaa \cdot CaM \cdot nCa^{2+}$$
$$NaIQ \cdot CaM + nCa^{2+} \rightarrow NaIQ \cdot CaM \cdot nCa^{2+}$$

The results that peptide·CaM complexes bind with Ca^{2+} at lower Ca^{2+} concentrations than CaM indicate that the peptide binding to CaM enhances the Ca^{2+} affinity of CaM. This implies that the binding of VDSC to CaM increases the Ca^{2+} sensitivity of CaM, which in turn couples with the conformational transition of the CaM·VDSC complex. Figure 17 illustrates a simple model for the interaction of peptides and CaM. There is a simple relationship of $K_d1K_d2=K_d3K_d4$. The overall average Ca^{2+} affinity of CaM (K_d1) is probably ~11 μM under physiological conditions (*48*). Since K_d2 and K_d3 were estimated experimentally, the equation leads to the estimation of K_d4 value being larger than K_d1 (>11 μM), suggesting that NaIQ·apoCaM has lower affinity for Ca^{2+} than apoCaM. However, NaIQ-dansyl-CaM complex showed a higher calcium sensitivity than that of CaM alone (Figure 11, solid triangle). The reason for the discrepancy between the measured and the estimated K_d4 value is not known. But I suspect that dansyl-CaM alone and dansyl-CaM in the NaIQ·CaM complex may emit fluorescence at different calcium binding ratios, because a danylated site is located at the middle position of CaM (far from Ca^{2+} binding domains). It is suggested that

the fluorescence of dansyl-CaM does not directly reflect the Ca^{2+}-binding ratio. Nevertheless, the controversial K_d4 value is very interesting phenomenon to study the process of the CaM complex formation.

What is the function of the CaM·VDSC complex? High-affinity CaM-target proteins (K_d2 ≤ 10 nM in figure 17) are thought to be activated efficiently throughout mammalian cells (*49*). In our results, K_d2 is 4.6 nM for NaIQ·Ca^{2+}CaM. I assume that this value is sufficiently small enough to cause functional interactions between CaM and VDSC in neuronal cells. The Ca^{2+} concentration where the state transition between NaIQ·apoCaM and NaIQ·Ca^{2+}CaM is halfway is 250 nM in the Ca^{2+} titration experiment (Figure 11, triangles). This Ca^{2+} concentration is higher than the basal Ca^{2+} level (about 100 nM), but is an easily attainable level when a train of action potentials is generated. In response to changes in intracellular Ca^{2+} concentration, the complex conformation will shift from apoCaM·VDSC to Ca^{2+}CaM·VDSC, and vice versa. Recent observations showed that direct binding of CaM, which acts as a Ca^{2+} sensor, modulates functions of several ion channels. Besides the Ca^{2+}-dependent binding, CaM is concentrated in nerve terminals through the apoCaM·GAP43 interaction in neuronal cells (*43*). In a similar way, interaction of CaM with the IQ-like motif in VDSC may be required to keep a sufficient CaM concentration in low Ca^{2+} conditions. I performed electrophysiological analysis to study the influence of conformation

change from apoCaM to Ca^{2+}CaM. Deletion of CBS of rBII (rBIIΔCBS) practically abolished the functional activity. The mutant protein S-tagC-termE4 showed strongly lowered binding with CaM-agarose in the presence of Ca^{2+} but no binding in the absence of Ca^{2+}. Therefore, the electrophysiological experiments using the wild-type and E4 mutant VDSCs were intended to study the interaction with apoCaM. I studied the activation, the inactivation, the time of recovery form inactivation, and extracellular divalent cationic effect , but the difference between WT and E4 mutant was not noticeable.

The functional significance of Ca^{2+}CaM binding to VDSC has remained to be elucidated. The amino acid sequences around Region 2, however, are well conserved among the VDSC α-subunits (Table 2), suggesting that regulation through CaM binding may be common mechanism for VDSC. Future work should be concerned to study the *in vivo* binding of CaM to VDSC, the functional view of the apoCaM complex to the Ca^{2+}CaM complex transition, and another types of VDSC, not only typeII.

Acknowledgments

I would like to express my sincere appreciation for Professor Kuniaki Nagayama. I thank Dr. Takashi Konno for the valuable discussion throughout this study and his help in CD experiments. I am also sincerely grateful to Professor Keiji Imoto for helpful suggestion and his help in electrophysiological experiments. I thank Professor Masaharu Noda for providing the voltage-dependent sodium channel typeII cDNA, Dr. Tatsuya Maeda for providing pAS2-1C plasmid, and Ms. Yumiko Makino (National Institute for Basic Biology, Center for Analytical Instruments) for operating the mass spectrometer and the protein sequencer.

References

1. Catterall, W. A. (1995): Structure and function of voltage-gated ion channels. *Annu. Rev. Biochem. 64*, 493–531.

2. Noda, M., Ikeda, T., Kayano, T., Suzuki, H., Takeshima, H., Kurasaki, M., Takahashi, H., and Numa, S. (1986): Existence of distinct sodium channel messenger RNAs in rat brain. *Nature 320*, 188–192.

3. Ma, J. Y., Catterall, W. A., and Scheuer, T. (1997): Persistent sodium currents through brain sodium channels induced by G protein betagamma subunits. *Neuron 19*, 443–452.

4. Srinivasan, Y., Elmer, L., Davis, J., Bennett, V., and Angelides, K. (1988): Ankyrin and spectrin associate with voltage-dependent sodium channels in brain. *Nature 333*, 177–180.

5. Tibbs, V. C., Gray, P. C., Catterall, W.A., and Murphy, B. J. (1998): AKAP15 anchors cAMP-dependent protein kinase to brain sodium channels. *J. Biol. Chem. 273*, 25783–25788.

6. Fields, S., and Song, O. (1989): A novel genetic system to detect protein-protein interactions. *Nature 340*, 245–246.

7. Nelson, M. R., and Chazin, W. J. (1998) in *Calmodulin and Signal Transduction* (Van Eldik, L. J., and Watterson, D. M., Eds.) pp 17–64, Academic Press, San Diego, CA.

8. Saimi, Y., and Ling, K. Y. (1990): Calmodulin activation of calcium-dependent sodium

channels in excised membrane patches of Paramecium. *Science 249*, 1441–1444.

9. Saimi, Y., and Kung, C. (1994): Ion channel regulation by calmodulin binding. *FEBS Lett. 350*, 155–158.

10. Grunwald, M. E., Yu, W. P., Yu, H. H., and Yau, K.W. (1998): Identification of a domain on the beta-subunit of the rod cGMP-gated cation channel that mediates inhibition by calcium-calmodulin. *J. Biol. Chem. 273*, 9148–9157.

11. Weitz, D., Zoche, M., Muller, F., Beyermann, M. Korschen, H. G, Kaupp, U. B., and Koch, K. W. (1998): Calmodulin controls the rod photoreceptor CNG channel through an unconventional binding site in the N-terminus of the beta-subunit. *EMBO J. 17*, 2273–2284.

12. Ehlers, M. D., Zhang, S., Bernhadt, J. P., and Huganir, R. L. (1996): Inactivation of NMDA receptors by direct interaction of calmodulin with the NR1 subunit. *Cell 84*, 745–755.

13. Xia, X. M., Fakler, B., Rivard, A., Wayman, G., Johnson-Pais, T., Keen, J. E., Ishii, T., Hirschberg, B., Bond, C. T., Lutsenko, S., Maylie, J., and Adelman, J. P. (1998): Mechanism of calcium gating in small-conductance calcium-activated potassium channels. *Nature 395*, 503–507.

14. Qin, N., Olcese, R., Bransby, M., Lin, T., and Birnbaumer, L. (1999): Ca2+-induced inhibition of the cardiac Ca2+ channel depends on calmodulin. *Proc. Natl. Acad. Sci.. U.*

S. A. 96, 2435–2438.

15. Peterson, B. Z., DeMaria, C. D., and Yue, D. T. (1999): Calmodulin is the Ca2+ sensor for Ca2+ -dependent inactivation of L-type calcium channels. *Neuron 22*, 549–558.

16. Zühlke, R. D., Pitt, G. S., Deissseroth, K., Tsein, R. W., and Reuter, H. (1999): Calmodulin supports both inactivation and facilitation of L-type calcium channels. *Nature 399*, 159–162.

17. Lee, A., Wong, S. T., Gallagher, D., Li, B., Storm, D. R., Scheuer, T., and Catterall, W. A. (1999): Ca2+/calmodulin binds to and modulates P/Q-type calcium channels. *Nature 399*, 155–159.

18. Stühmer, W., Conti F., Suzuki, H., Wang, X. D., Noda, M., Yahagi, N., Kubo, H., and Numa, S. (1989): Structural parts involved in activation and inactivation of the sodium channel. *Nature 339*, 597–603.

19. Shinobu, N., Maeda, T., Aso, T., Ito, T., Kondo, T., Koike, K., and Hatakeyama, M. (1999): Physical interaction and functional antagonism between the RNA polymerase II elongation factor ELL and p53. *J. Biol. Chem. 274*, 17003–17010.

20. Studier, F. W. (1991): Use of bacteriophage T7 lysozyme to improve an inducible T7 expression system. *J. Mol. Biol. 219*, 37–44.

21. LaVallie, E. R., DiBlasio, E. A., Kovacic, S., Grant, K. L., Schendel, P. F., and McCoy, J. M. (1993): A thioredoxin gene fusion expression system that circumvents inclusion body

formation in the E. coli cytoplasm. *Bio/Technology 11*, 187–193.

22. Gopalakrishna, R., and Anderson, W. B. (1982): Ca^{2+}-induced hydrophobic site on calmodulin: application for purification of calmodulin by phenyl-Sepharose affinity chromatography. *Biochem. Biophys. Res. Commun. 104,* 830–836.

23. Vorherr, T., James, P., Krebs, J., Enyedi, A., McCormick, D. J., Penniston, J. T., Carafoli, E. (1990): Interaction of calmodulin with the calmodulin binding domain of the plasma membrane Ca2+ pump. *Biochemistry 29,* 355–365.

24. Chen, R. F. (1968): Dansyl labeled proteins: determination of extinction coefficienc and number of bound residues with radioactive dansyl chloride. *Anal. Biochem. 25*, 412–416.

25. Press, W. H., Flanney, B. P., Teukolsky, S. A., Vetterling, W. T. (1988) *Numerical Recipes in C*, Cambridge University Press, UK.

26. Schwarzenbach, G., Senn, H., and Anderegg, G. (1957) *Helv. Chim. Acta 40*, 1886–1900

27. Dedman, J. R., Jackson, R. L., Schreiber, W. E., and Means, A. R. (1978): Sequence homology of the Ca2+-dependent regulator of cyclic nucleotide phosphodiesterase from rat testis with other Ca2+-binding proteins. *J. Biol. Chem. 253*, 343–346.

28. O'Neil, K. T., and DeGrado, W. F. (1990): How calmodulin binds its targets: sequence independent recognition of amphiphilic alpha-helices. *Trends. Biochem. Sci. 15*, 59–64.

29. Cheney, R. E., and Mooseker, M. S. (1992): Unconventional myosins. *Curr. Opin. Cell Biol. 4*, 27–35.

30. Rhoads, A. R., and Friedberg, F. (1997): Sequence motifs for calmodulin recognition. *FASEB J. 11*, 331–340.

31. Yeh, S. W., Ong, L. J., Clark, J. H., Glazer, A. N. (1987): Fluorescence properties of allophycocyanin and a crosslinked allophycocyanin trimer. *Cytometry 8*, 91-95

32. Afshar, M., Caves, L. S., Guimard, L., Hubbard, R. E., Calas, B., Grassy, G., Haiech, J. (1994): Investigating the high affinity and low sequence specificity of calmodulin binding to its targets. *J. Mol. Biol. 244*, 554-571

33. Olwin, B. B., and Storm, D. R. (1983): Preparation of fluorescent labeled calmodulins. *Methods in Enzymol. 102*, 148–157.

34. Torok, K., Cowley, D. J., Brandmeier, B. D., Howell, S., Aitken, A., and Trentham, D. R. (1998) : Inhibition of calmodulin-activated smooth-muscle myosin light-chain kinase by calmodulin-binding peptides and fluorescent (phosphodiesterase-activating) calmodulin derivatives. *Biochemistry 37*, 6188–6198.

35. Wriggers, W., Mehler, E., Pitici, F., Weinstein, H., and Schulten, K. (1998): Structure and dynamics of calmodulin in solution. *Biophys J. 74*, 1622–1639.

36. Kuboniwa, H., Tjandra, N., Grzesiek, S., Ren, H., Klee, C. B., and Bax, A. (1995): Solution structure of calcium-free calmodulin. *Nat. Struct. Biol. 2*, 768–776.

37. Klevit, R. E. (1983): Spectroscopic analyses of calmodulin and its interactions. *Methods in Enzymol. 102*, 82–104.

38. Comte, M., Maulet, Y., and Cox, J. A.(1983): Ca^{2+}-dependent high-affinity complex formation between calmodulin and melittin. *Biochem J. 209*, 269–272.

39. Scaloni, A., Miraglia, N., Orru, S., Amodeo, P., Motta, A., Marino, G., and Pucci, P. (1998): Topology of the calmodulin-melittin complex. *J. Mol. Biol. 277*, 945–958.

40. Chattopadhyaya, R., Meador, W. E., Means, A. R., Quiocho, F. A. (1992): Calmodulin structure refined at 1.7 A resolution. *J. Mol. Biol. 228*, 1177–1192.

41. Zhang, M., Tanaka, T., and Ikura, M. (1995): Calcium-induced conformational transition revealed by the solution structure of apo calmodulin. *Nat. Struct. Biol. 2*, 758–767.

42. Hanley, R. M., Means, A. R., Ono, T., Kemp, B. E., Burgin, K. E., Waxham, N., and Kelly, P. T. (1987): Mapping of calmodulin-binding domain of Ca2+/calmodulin-dependent protein kinase II from rat brain. *Science 237*, 293–297.

43. Blumenthal, D. K., Charbonneau, H., Edelman, A. M., Hinds, T. R., Rosenberg, G. B., Storm, D. R., Vincenzi, F. F., Beavo, J. A., and Krebs, E. G. (1988): Synthetic peptides based on the calmodulin-binding domain of myosin light chain kinase inhibit activation of other calmodulin-dependent enzymes. *Biochem. Biophys. Res. Commun. 156*, 860–865.

44. Cimler, B. M., Andreasen, T. J., Andreasen, K. I., and Storm, D. R. (1985): P-57 is a neural specific calmodulin-binding protein. *J. Biol. Chem. 260*, 10784–10788.

45. Alexander, K. A., Wakim, B. T., Doyle, G.S., Walsh, K. A., and Storm, D. R., (1988):

Identification and characterization of the calmodulin-binding domain of neuromodulin, a neurospecific calmodulin-binding protein. *J. Biol. Chem. 263*, 7544–7549.

46. Ikura, M., Clore, G. M., Gronenborn, A. M., Zhu, G., Klee, C. B., Bax, A. (1992): Solution structure of a calmodulin-target peptide complex by multidimensional NMR. *Science 256*, 632–638.

47. Urbauer, J. L, Short, J. H., Dow, L. K., and Wand, A. J. (1995): Structural analysis of a novel interaction by calmodulin: high-affinity binding of a peptide in the absence of calcium. *Biochemistry 34*, 8099–8109.

48. Cox, J. A. (1988): Interactive properties of calmodulin. *Biochem. J.* 249, 621-629

49. Persechini, A., and Cronk, B. (1999): The relationship between the free concentrations of Ca^{2+} and Ca^{2+}-calmodulin in intact cells. *J. Biol. Chem. 274*, 6827–6830.

50. Kayano, T., Noda, M., Flockerzi, V., Takahashi, H., and Numa, S. (1988): Primary structure of rat brain sodium channel III deduced from the cDNA sequence. *FEBS Lett. 228*, 187–194.

51. Dietrich, P. S., McGivern, J. G., Delgado, S. G., Koch, B. D., Eglen, R. M., Hunter, J. C., and Sangameswaran, L. (1998): Functional analysis of a voltage-gated sodium channel and its splice variant from rat dorsal root ganglia. *J. Neurochem. 70*, 2262–2272.

Table 1: Summary of the results on peptide-CaM binding.

Peptide-CaM	Gel mobility shift assay[a]	Fluorescence spectroscopy[b]		CD spectroscopy[c]
	Peptide : CaM	K_d	Increment (480 nm)	Increment (222 nm)
NaIQ-Ca^{2+}CaM	4 : 1	4.6 nM (K_d2)	93%	enhanced
NaBaa-Ca^{2+}CaM	<4 : 1	89.7 nM (K_d2)	114%	n.d.
NaIQ-apoCaM	2 : 1	n.d.	7%	enhanced
NaBaa-apoCaM	no shift	n.d.	3%	n.d.

[a]Peptide-to-CaM ratio where complete shift was observed. "no shift" indicates that no complex was detected. [b]Dissociation constants (K_d) of peptides for CaM and increments of fluorescence intensity (480 nm) induced by peptides. K_d2 is indicated by figure 18. [c]Changes in negative ellipticity induced by peptides. n.d. = not determined

Table 2: Alignment of the IQ-like motif in the C-terminal of VDSC typeII with other VDSC proteins and CaM binding proteins containing IQ motifs.

VDSC typeII(NaIQ,rat)	KRKQEEVSAIVIQRAYRRYLLKQKVKK
VDSC typeIII (rat)	KRKQEEVSAAIIQRNYRCYLLKQRLKN
VDSC rPN4 (rat)	RRKQEEVSAVVLQRAYRGHLARRGFIC
L-type VDCC (human)	VTVGKFYATFLIQEYFRKFKKRKEQGL
CNG β-subunit (bovine)	ASTNSAIINDRLQELVKLFKERTEKVK
Myosin I (chicken)	RQQRVAELATLIQKMFRGWCCRKRYQL
GAP-43 (human)	PEDKAHKAATKIQASFRGHITRKKLKG

Shaded characters indicate the IQ motif consensus sequence. Single underlined and double underlined residues represent a homologous and identical residue of NaIQ. VDSC typeIII (*50*), rPN4 (*51*), L-type VDCC (*16*), CNG β-subunit (*11*), Myosin I (*29*), GAP-43 (*44*).

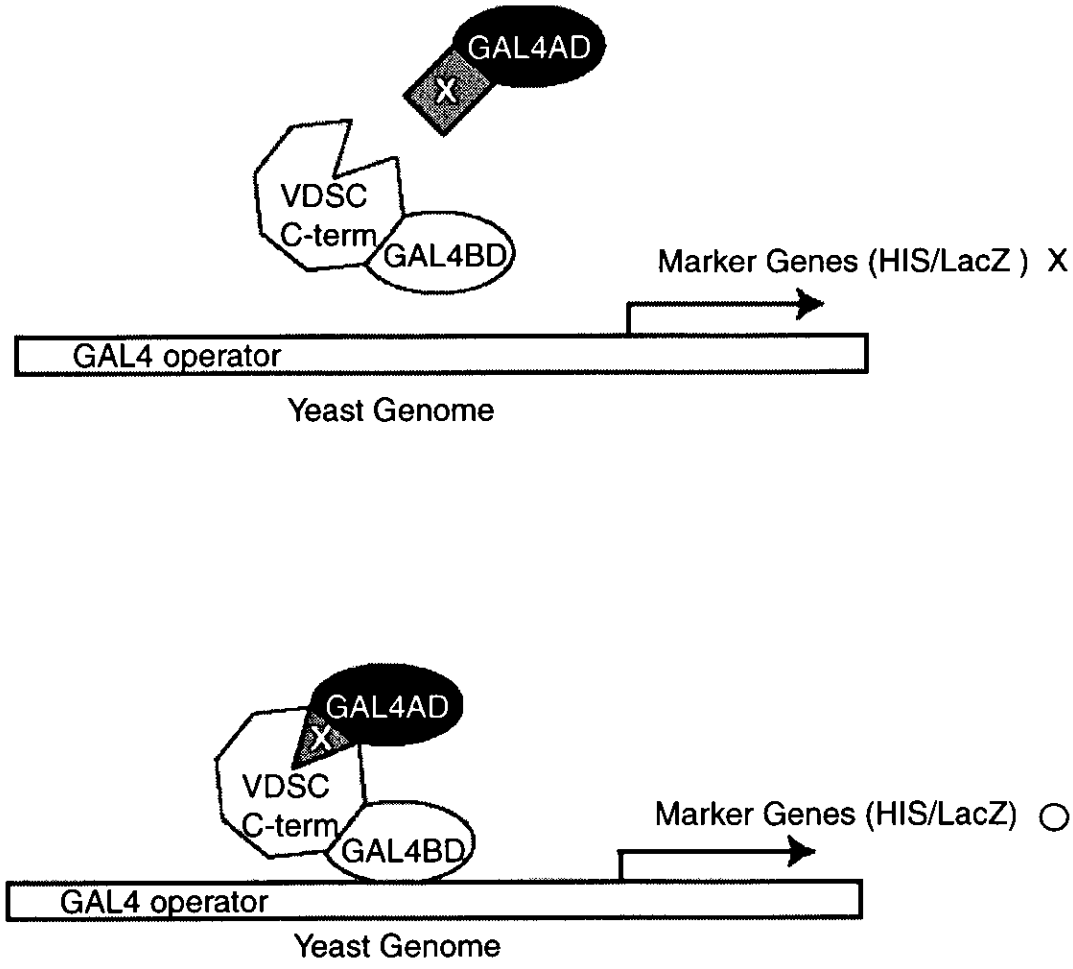
GAL4AD
X
VDSC
C-term
GAL4BD
Marker Genes (HIS/LacZ) X
GAL4 operator
Yeast Genome
GAL4AD
X
VDSC
C-term
GAL4BD
Marker Genes (HIS/LacZ) ○
GAL4 operator
Yeast Genome

Figure 1

Figure 1: ***Scheme of the GAL4-based Two-Hybrid system***

The cDNA of the target protein (the C-terminal domain of the VDSC) is inserted into the GAL4 DNA-BD plasmid (pAS2-1), and cDNAs of candidate interacting protein (from rat brain library) are inserted into the GAL4 AD plasmid. The recombinant plasmids are cotransformed into a reporter yeast strain Y190. Y190 cells possess the HIS3 and lacz genes under control of a GAL4 responsive element. The HIS3 gene allows a positive growth selection for clones that are transformed by two interacting hybrid constructs, and blue screening (β-galactosidase activity) is then used to further confirm the interaction. (upper; non-interactive, lower; interactive)

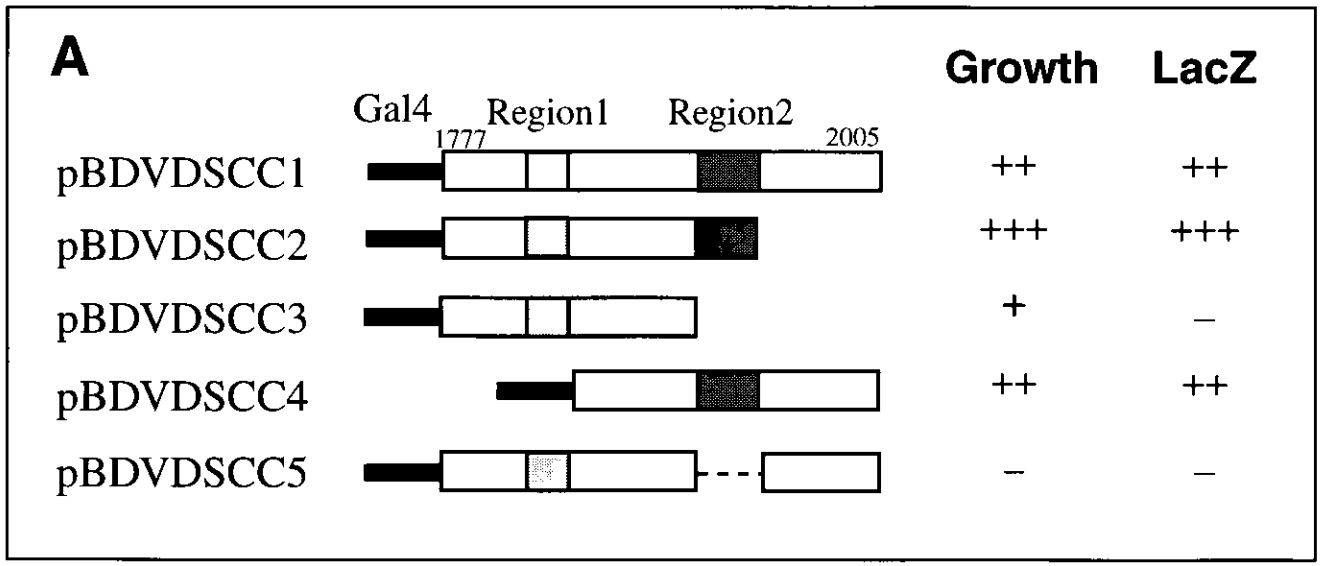
A
Growth
LacZ
Gal4
Region1
Region2
1777
2005
pBDVDSCC1
++
++
pBDVDSCC2
+++
+++
pBDVDSCC3
+
–
pBDVDSCC4
++
++
pBDVDSCC5
–
–

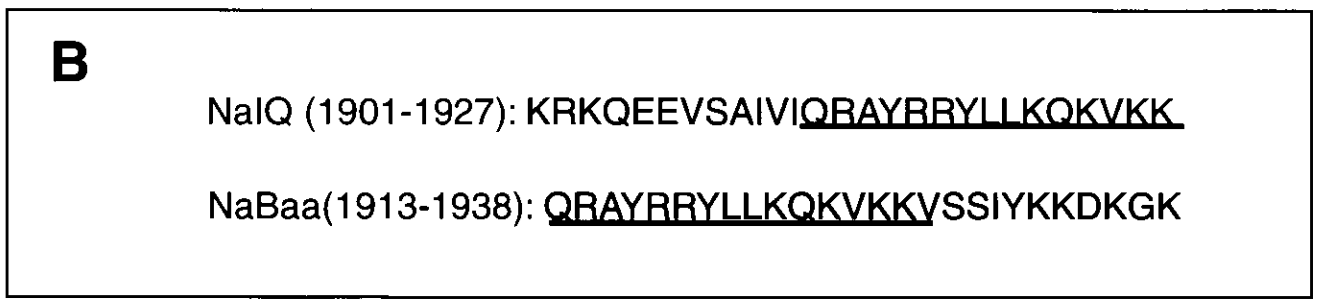
B
NalQ (1901-1927): KRKQEEVSAIVIQRAYRRYLLKQKVKK
NaBaa(1913-1938): QRAYRRYLLKQKVKKVSSIYKKDKGK

Figure 2

Figure 2: ***Constructs for wild-type and mutated VDSC C-terminal domains used in the two-hybrid interaction assay and the result***

(A); The Gal4 sequence (thick solid line) was fused with the wild-type or deleted sequences encoding of the C-terminal domain (boxes). Putative CaM binding sites, Region 1 and Region 2, are indicated by light and dark shaded boxes, respectively. The dashed line indicates deletion of Region 2. Growth of yeast incubated 5 days after cotransfection. Cell growth of yeast was observed on the selection plate, and LacZ activity studied using β-galactosidase assay. – None, + Weak, + + Moderate, and + + + Strong. (B); Amino acid sequence of synthetic peptides (NaIQ: 1901—1927 aa and NaBaa: 1913—1938), which derived from Region2 (1901-1938 aa, renamed as CBS). The underlines are the over lapped sequence in both peptides.

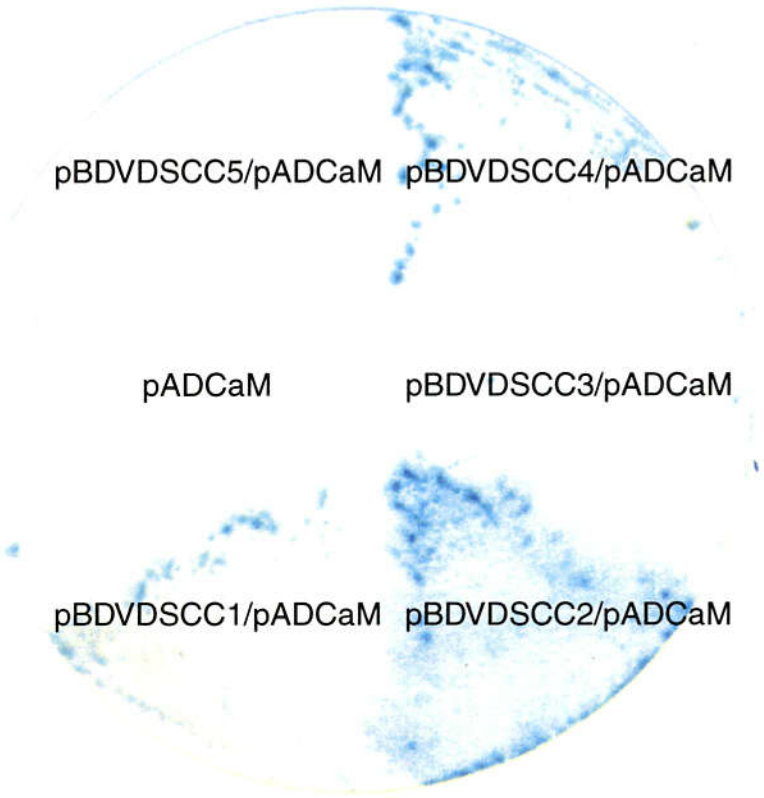
pBDVDSCC5/pADCaM
pBDVDSCC4/pADCaM
pADCaM
pBDVDSCC3/pADCaM
pBDVDSCC1/pADCaM
pBDVDSCC2/pADCaM

Figure 3

Figure 3: ***Demonstration of the blue reaction of β-galactosidase activity with plasmids encoding wild or mutated C-terminal domains***

Strain Y190 cells were transformed with pBDVDSCs together with pADCaM. Transformants were incubated either on a SD/-Trp/-Leu/-His/+3-AT plate, which not only selects for the presence of the plasmids, also selects for transcriptional activation of HIS3 reporter gene (colony). Furthermore, only the combination of pBDVDSCC1(WT), pBDVDSCC2, pBDVDSCC4 and pADCaM demonstrated β-galactosidase activity.

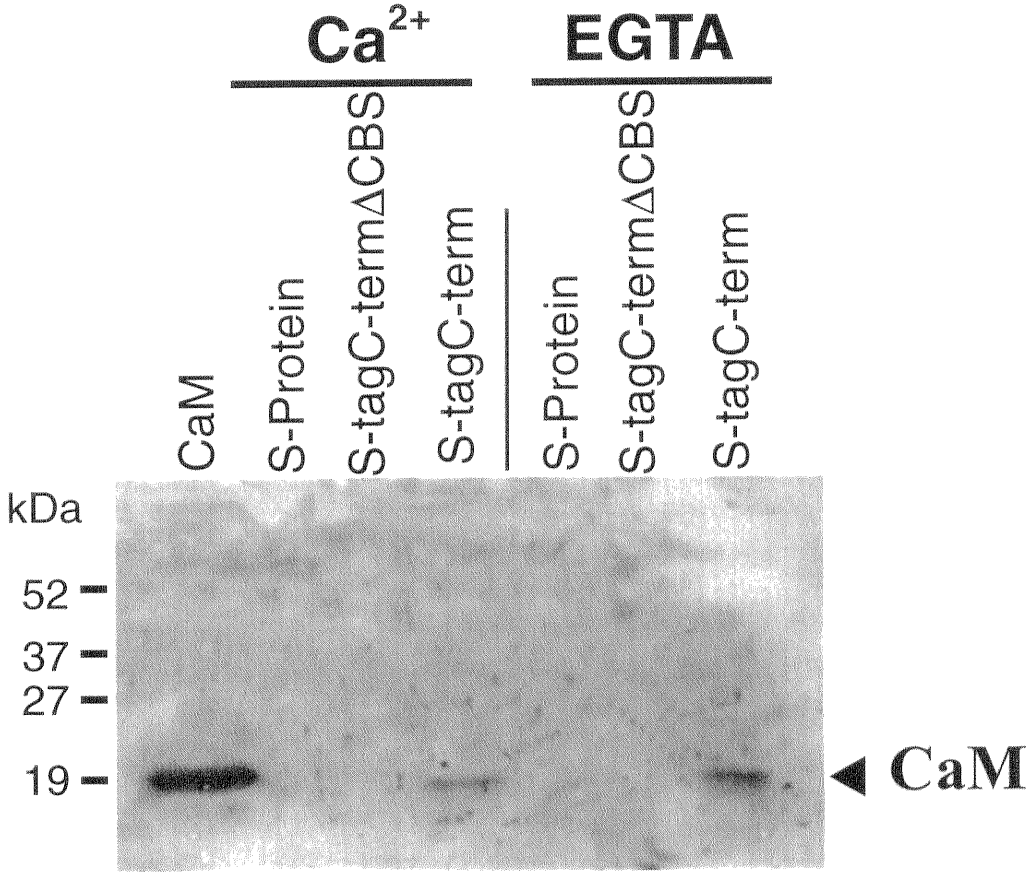
Ca2+
EGTA
CaM
S-Protein
S-tagC-termΔCBS
S-tagC-term
S-Protein
S-tagC-termΔCBS
S-tagC-term
kDa
52
37
27
19
CaM

Figure 4

Figure 4: ***Pull-down assay.***

The S-tag protein of the C-terminal domain of VDSC (S-tagC-term) or CBS deletion (S-tagC-termΔCBS) (10 μg of each) was incubated with S-protein agarose (50 μL) and rat brain extracts (100 μg of protein) in the presence of Ca^{2+} (0.5 mM) or EGTA (2 mM). The "S-protein" did not contain fusion proteins in the mixture. After washing by brief centrifugation, the pellets were solubilized with 50 μL of a SDS-PAGE sample buffer. CaM was detected by immunoblot analysis using an anti-CaM monoclonal antibody. CaM (10 ng) was run as a control.

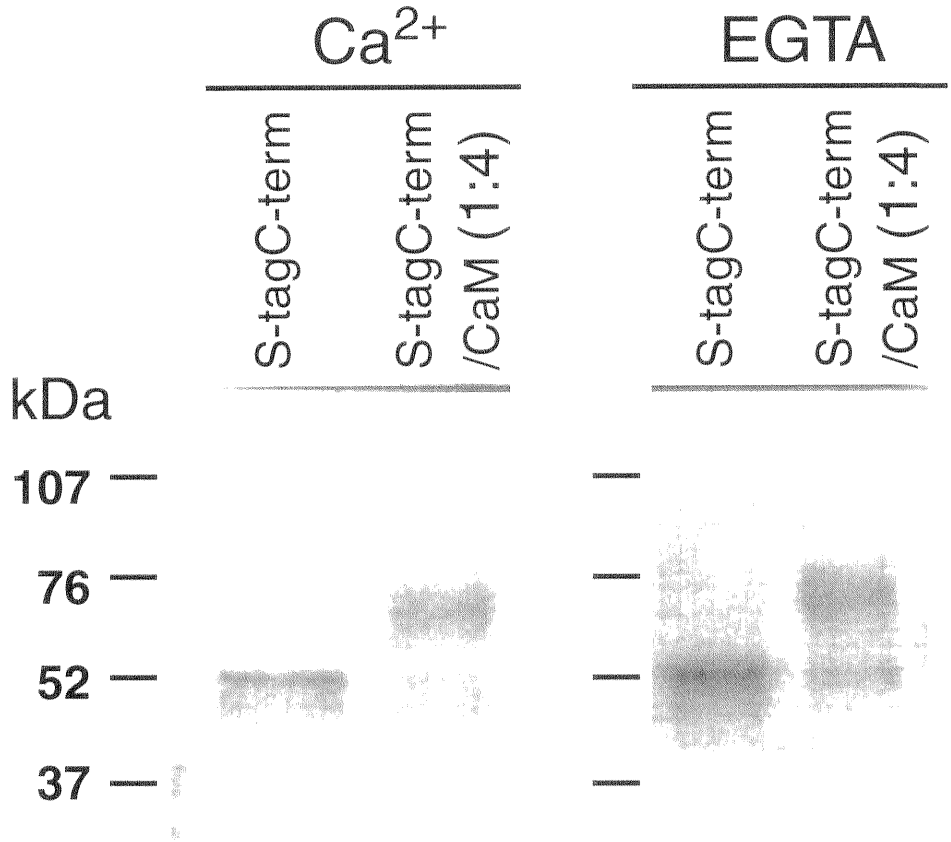
Ca2+
EGTA
S-tagC-term
S-tagC-term /CaM (1:4)
S-tagC-term
S-tagC-term /CaM (1:4)
kDa
107
76
52
37

Figure 5

Figure 5: ***Chemical cross linking.***

S-tag protein(S-tagC-term) alone or rat CaM were incubated in 200 μL of 50 mM Mes-HCl pH 7.0 and then treated with 750 μM of 1-ethyl-3(3-dimethylaminopropyl)carbodiimide (EDAC). Each sample applied to a 12.5% SDS-PAGE. After electrophoresis, the gel was electroblotted onto a nitrocellulose membrane. Fusion protein was detected by an alkalinephospatase-labelled S-protein (Novagen), and visualized by chemiluminescence (NEN).

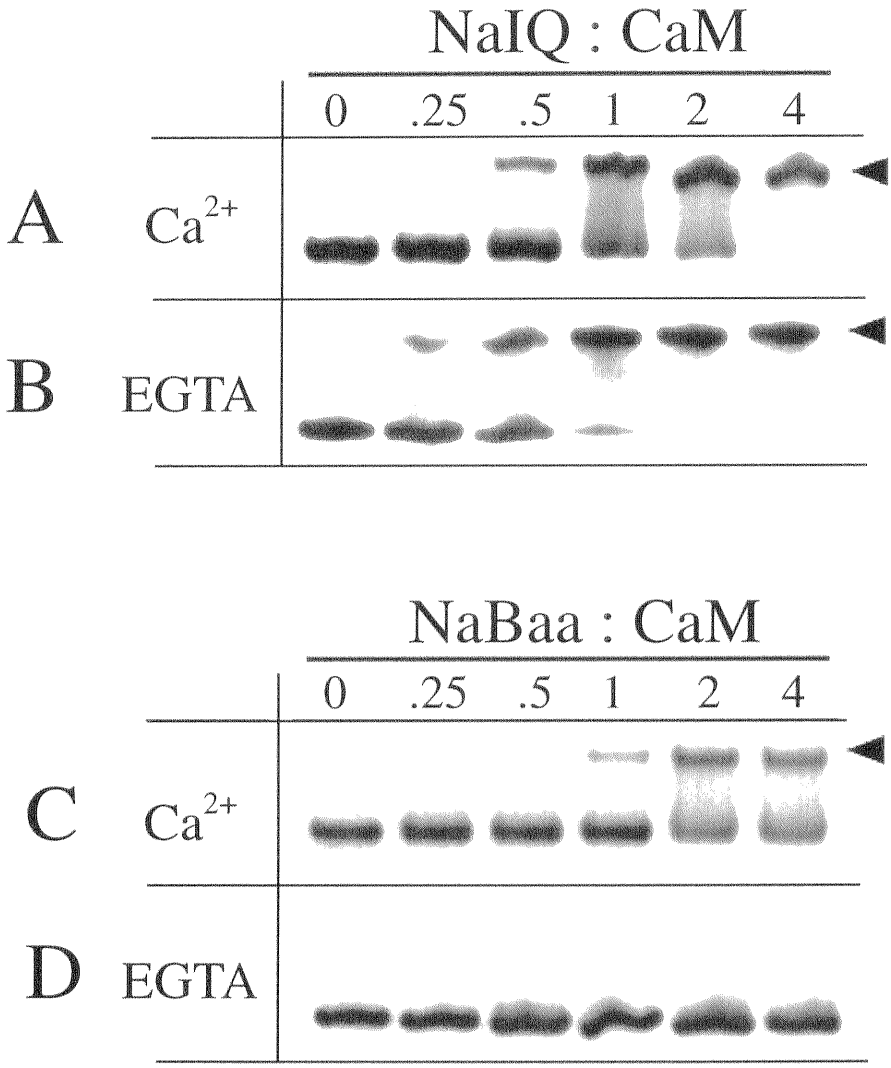

Figure 6

Figure 6: ***Gel mobility shift assay.***

CaM (2 μM) was incubated with NaIQ (A, B) or NaBaa (C, D) at different molar ratios in the presence of Ca^{2+} (1 mM $CaCl_2$; A, C) or in the absence of Ca^{2+} (2 mM EGTA; B,D). Each gel was visualized by silver staining. Arrowheads indicate the band of the peptide·CaM complex.

Figure 7: ***Changes in the dansyl-CaM fluorescence spectrum induced by peptides NaIQ (A) and NaBaa (B)***

Emission spectrum of dansyl-CaM (120 nM) alone (dotted lines), and mixtures of dansyl-CaM (120 nM) and peptides (300 nM) (solid lines) in 1 mM Ca^{2+} (red) or 2 mM EGTA (blue). Exitation was at 340 nm, and both exitation and emission slits were set at 10-nm band pass.

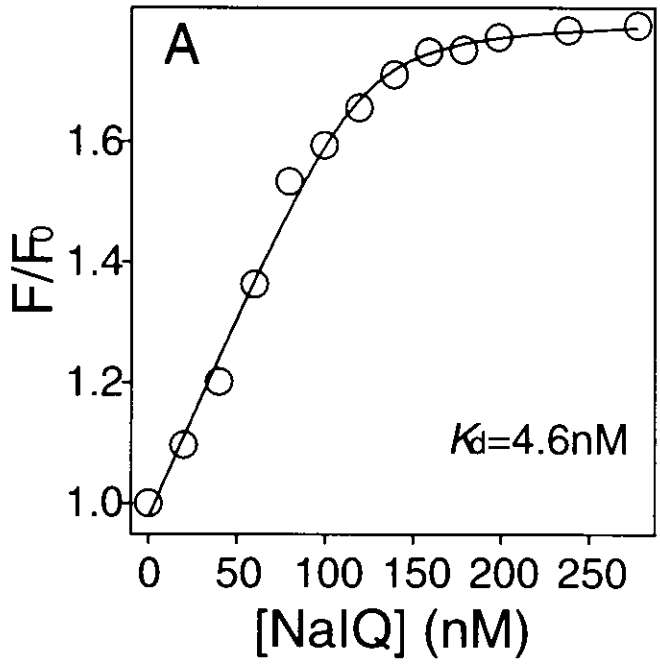
A
1.6
1.4
1.2
1.0
F/F0
Kd=4.6nM
0
50
100
150
200
250
[NalQ] (nM)

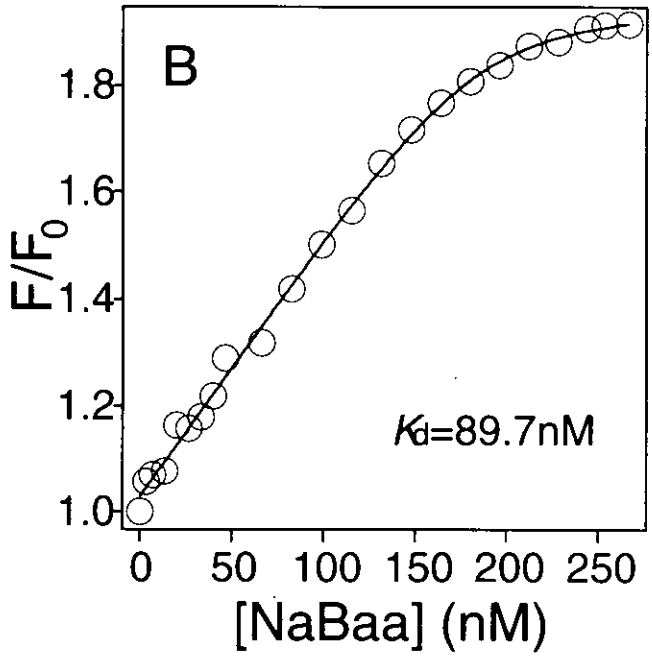
B
1.8
1.6
1.4
1.2
1.0
F/F0
Kd=89.7nM
0
50
100
150
200
250
[NaBaa] (nM)

Figure 8

Figure 8: ***Determination of the dissociation constant for the interaction CaM with peptides in the presence of*** Ca^{2+}.

The dansyl-CaM was titrated with addition of the VDSC peptides, (A) NaIQ, (B) NaBaa. The line is fitted by under Materials and Methods. The dissociation constant (K_d2 in figure 17) was 4.6 nM for NaIQ and 89.7 nM for NaBaa.

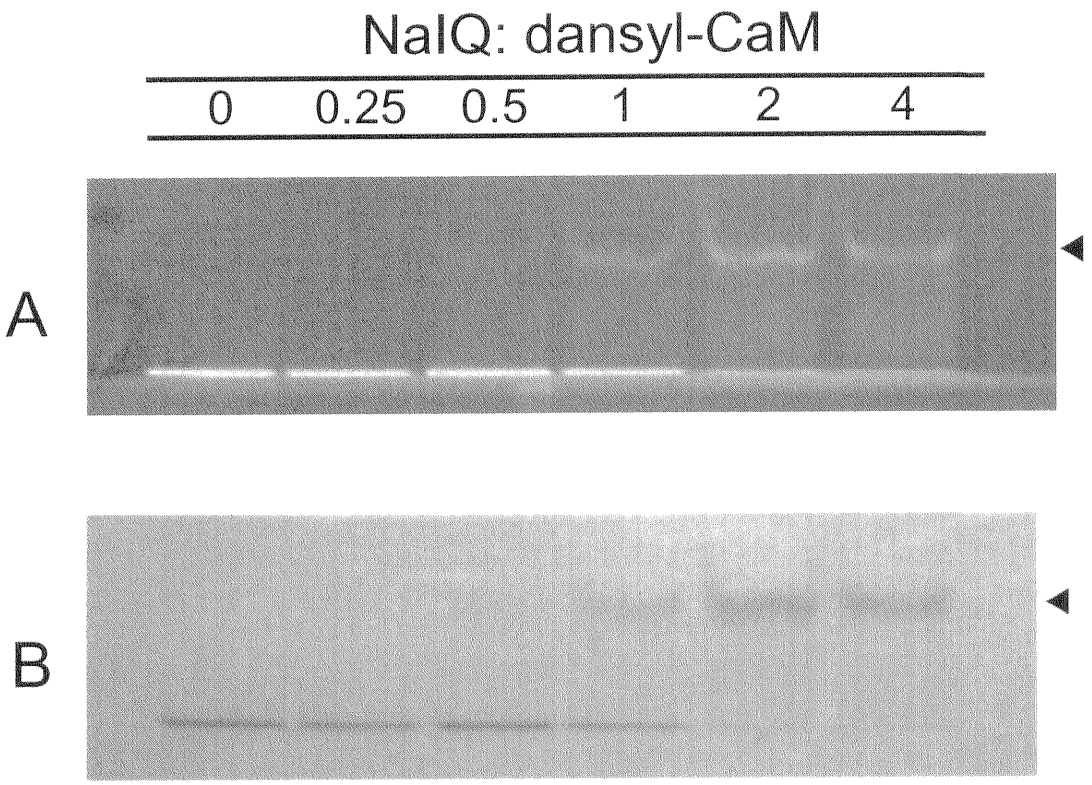

Figure 9

Figure 9: ***Gel mobility shift assay with dansyl-CaM.***

Dansyl-CaM (2 μM) was incubated with NaIQ at different molar ratios in the absence of Ca^{2+} (2 mM EGTA). (A) The gel was visualized by the Epi-Light UV detector (FA1100, Aisin Co., Ex 312 nm, fluorescence filtered from 400 to 550 nm). To stain the total protein, Coomassie Brilliant Blue visualized the same gel (B). Arrowheads indicate the band of the peptide·CaM complex.

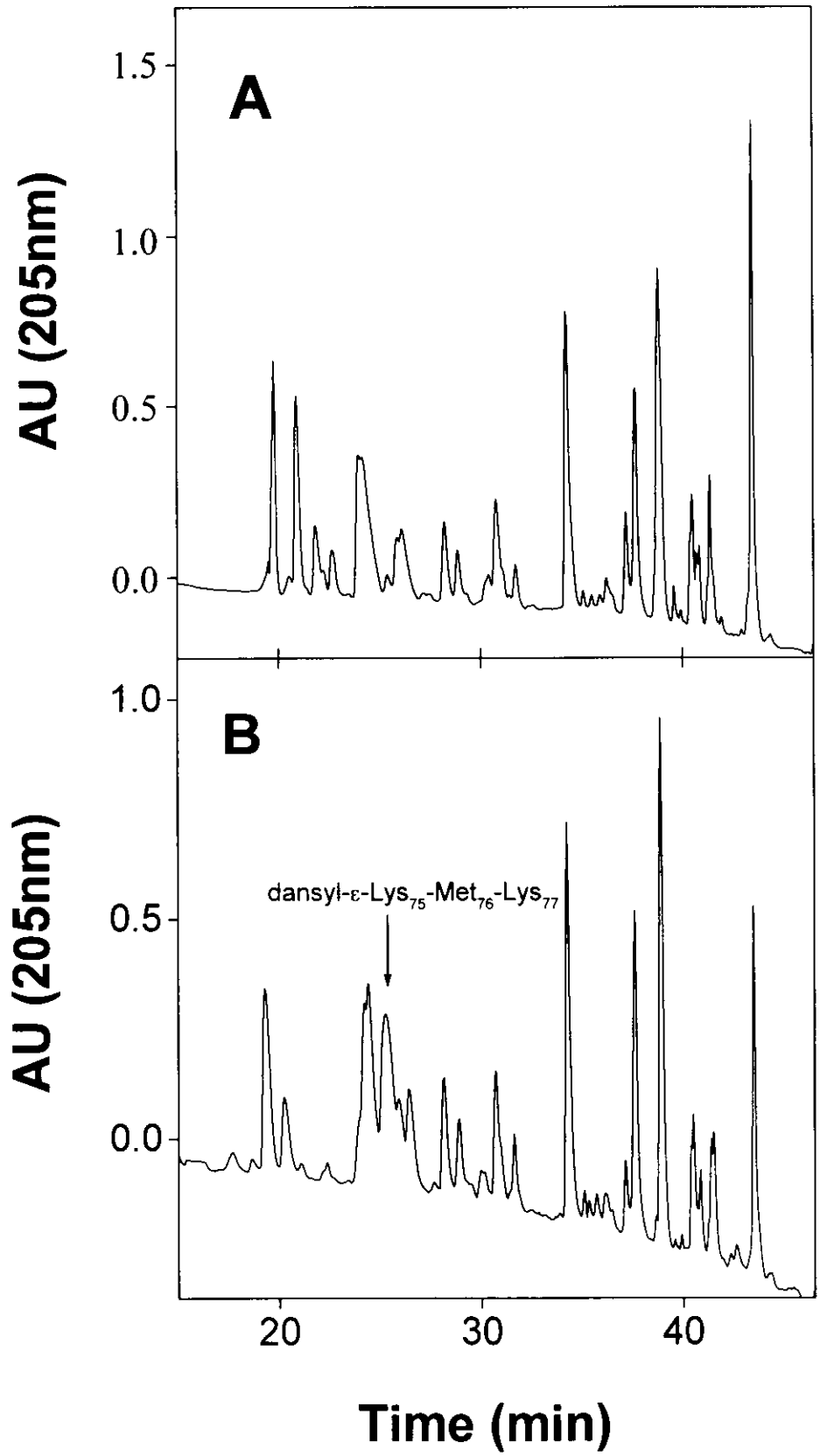
A
B
AU (205nm)
AU (205nm)
1.5
1.0
0.5
0.0
1.0
0.5
0.0
dansyl-ε-Lys75-Met76-Lys77
20
30
40
Time (min)

Figure 10

Figure 10: ***Tryptic digests of native CaM and dansyl-CaM.***

Separation of tryptic digests of rat brain CaM (A) and dansyl-CaM (B) by HPLC. Tryptic digests of CaM and dansyl-CaM (each 50 μg) were separated on a SMART system with a μRPC C2/C18 column (54 x 3 mm). The mobile phase was 0.1% trifluoroacetic acid with an increasing gradient of 0-50% acetonitrile as described under Materials and Methods. The arrow refers to peaks present in the HPLC profile of trypsin-digested dansyl-CaM peaks not present in the CaM profiles. Furthermore, this peak was found to contain more than 80 % of total fluorescence intensity.

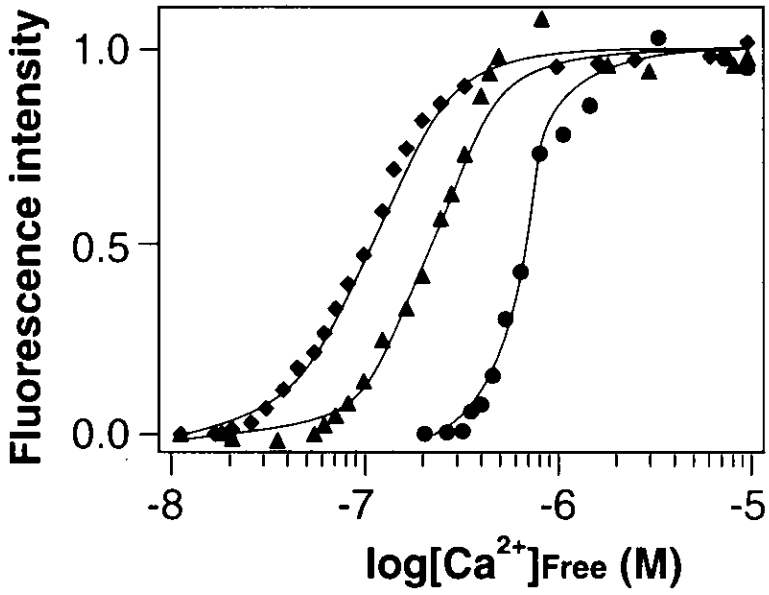

Figure 11

Figure 11: ***Ca^{2+}-dependency of dansyl-CaM fluorescence with or without peptides.***

Normalized fluorescence is shown for CaM (●), NaIQ-CaM mixture (▲), and NaBaa-CaM mixture (◆) under assay conditions described under Materials and Methods. Sigmoidal curves are just for visualization.

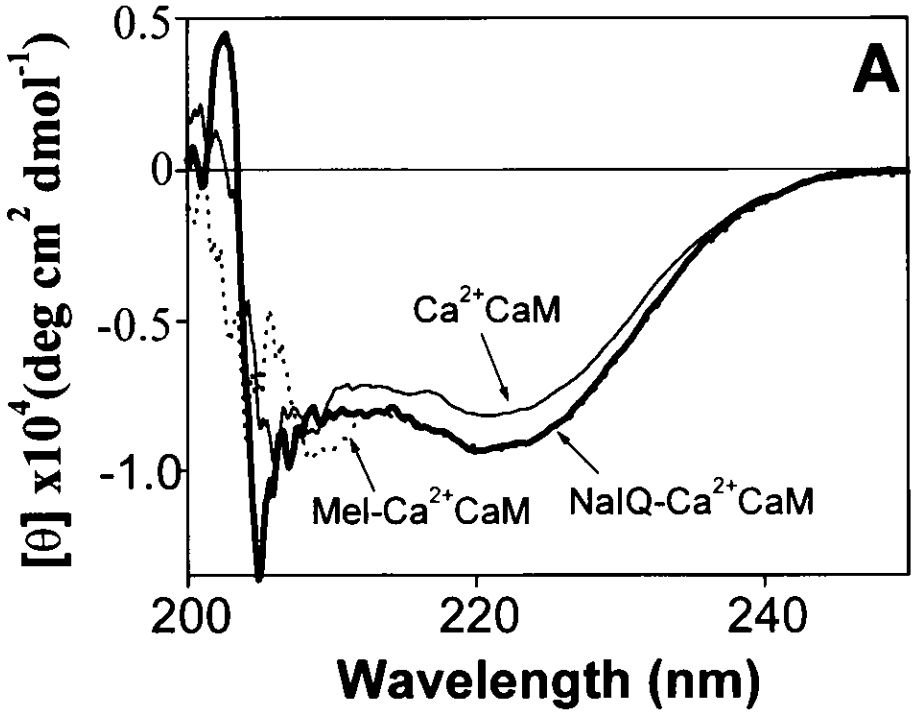
A
0.5
0
-0.5
-1.0
[θ] x10^4(deg cm^2 dmol^-1)
Ca2+CaM
Mel-Ca2+CaM
NalQ-Ca2+CaM
200
220
240
Wavelength (nm)

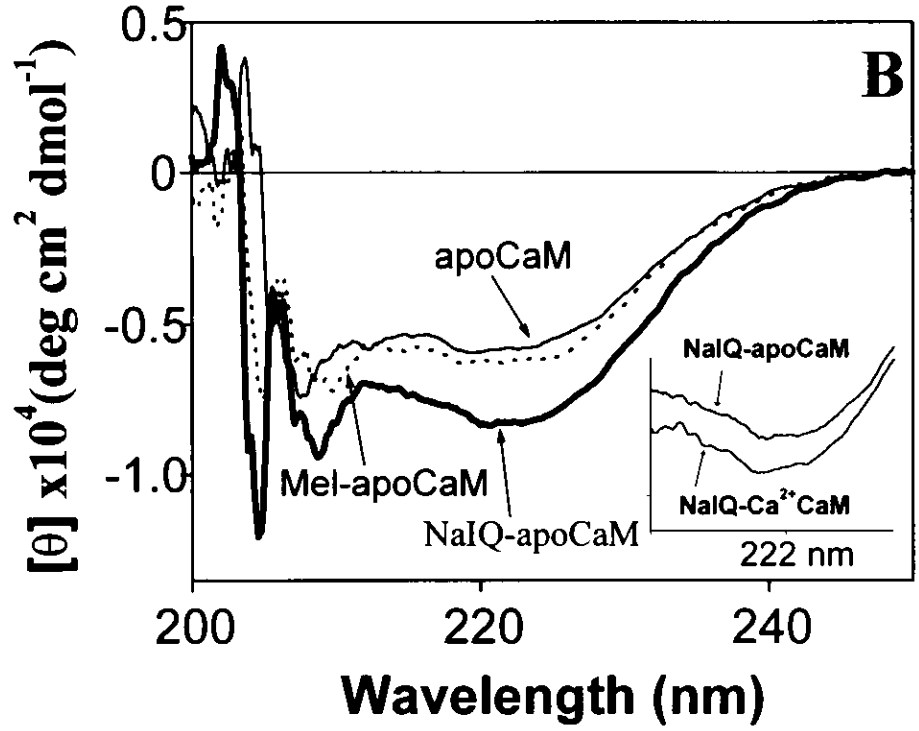
B
0.5
0
-0.5
-1.0
[θ] x10^4(deg cm^2 dmol^-1)
apoCaM
Mel-apoCaM
NalQ-apoCaM
NalQ-apoCaM
NalQ-Ca2+CaM
222 nm
200
220
240
Wavelength (nm)

Figure 12

Figure 12: ***CD spectra of CaM and peptide-CaM mixtures.***

CD spectra of CaM alone (thin solid lines), NaIQ-CaM mixture (thick solid lines), and melittin-CaM mixture (dotted lines) in the presence (A) or absence (B) of Ca^{2+}. Inset in panel B: CD spectra around 222 nm of NaIQ-Ca^{2+}CaM and NaIQ-apoCaM. The vertical and horizontal axes are on the same scale in A, B, and the inset.

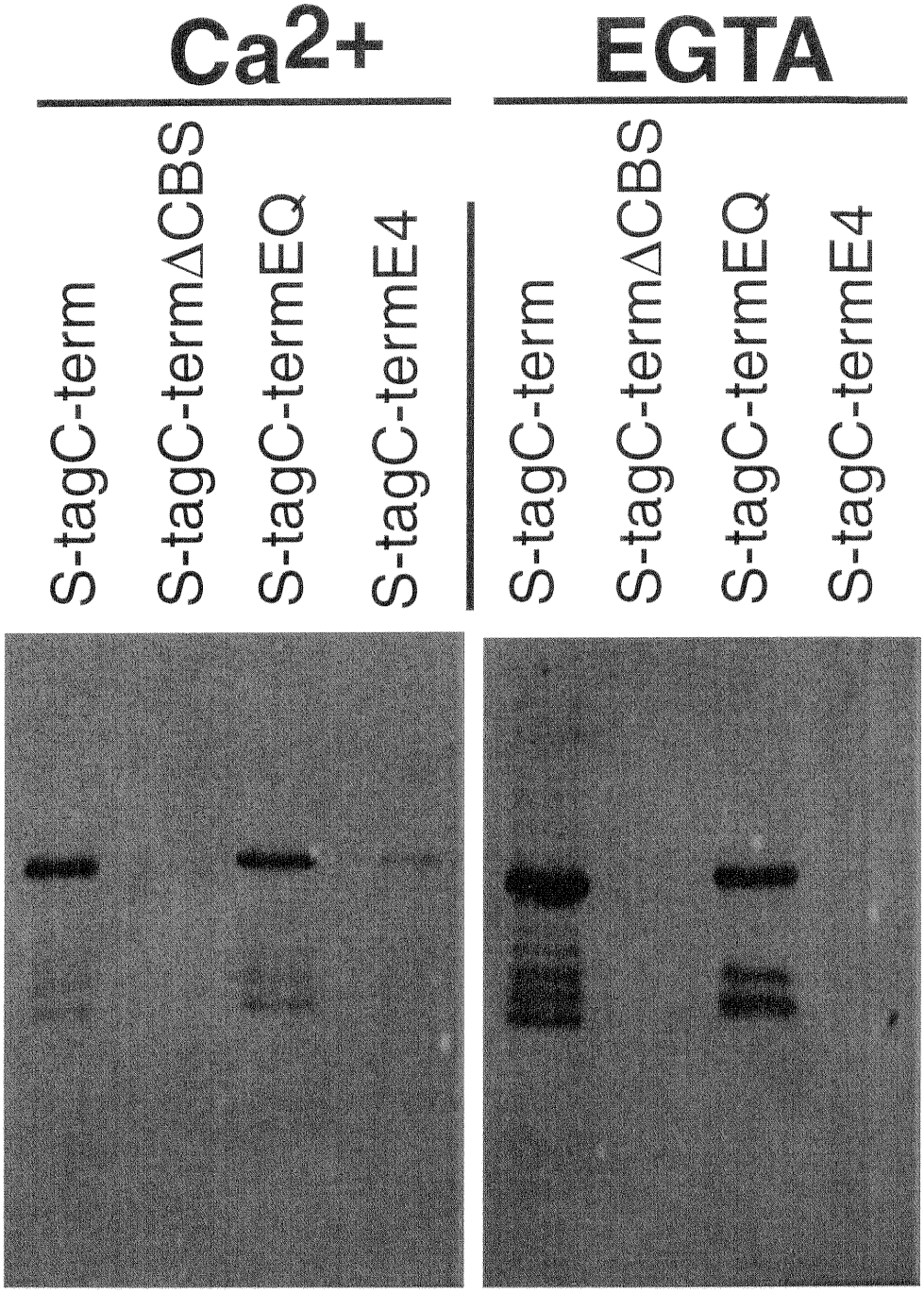
Ca2+
EGTA
S-tagC-term
S-tagC-termΔCBS
S-tagC-termEQ
S-tagC-termE4
S-tagC-term
S-tagC-termΔCBS
S-tagC-termEQ
S-tagC-termE4

Figure 13

Figure 13: ***CaM-agarose binding assay.***

The S-tag protein of the C-terminal domain of VDSC (S-tagC-term), CBS deleted protein (S-tagC-termΔCBS), I1912E mutant protein (S-tagC-termEQ), and E4 mutant protein (S-tagC-termE4) (10 μg of each) was incubated with CaM-agarose (50 μL) in the presence of Ca^{2+} (0.5 mM) or EGTA (2 mM). After washing by brief centrifugation, the pellets were solubilized with 50 μL of a SDS-PAGE sample buffer. S-tag protein was detected by an alkalinephosphatase conjugated S-protein.

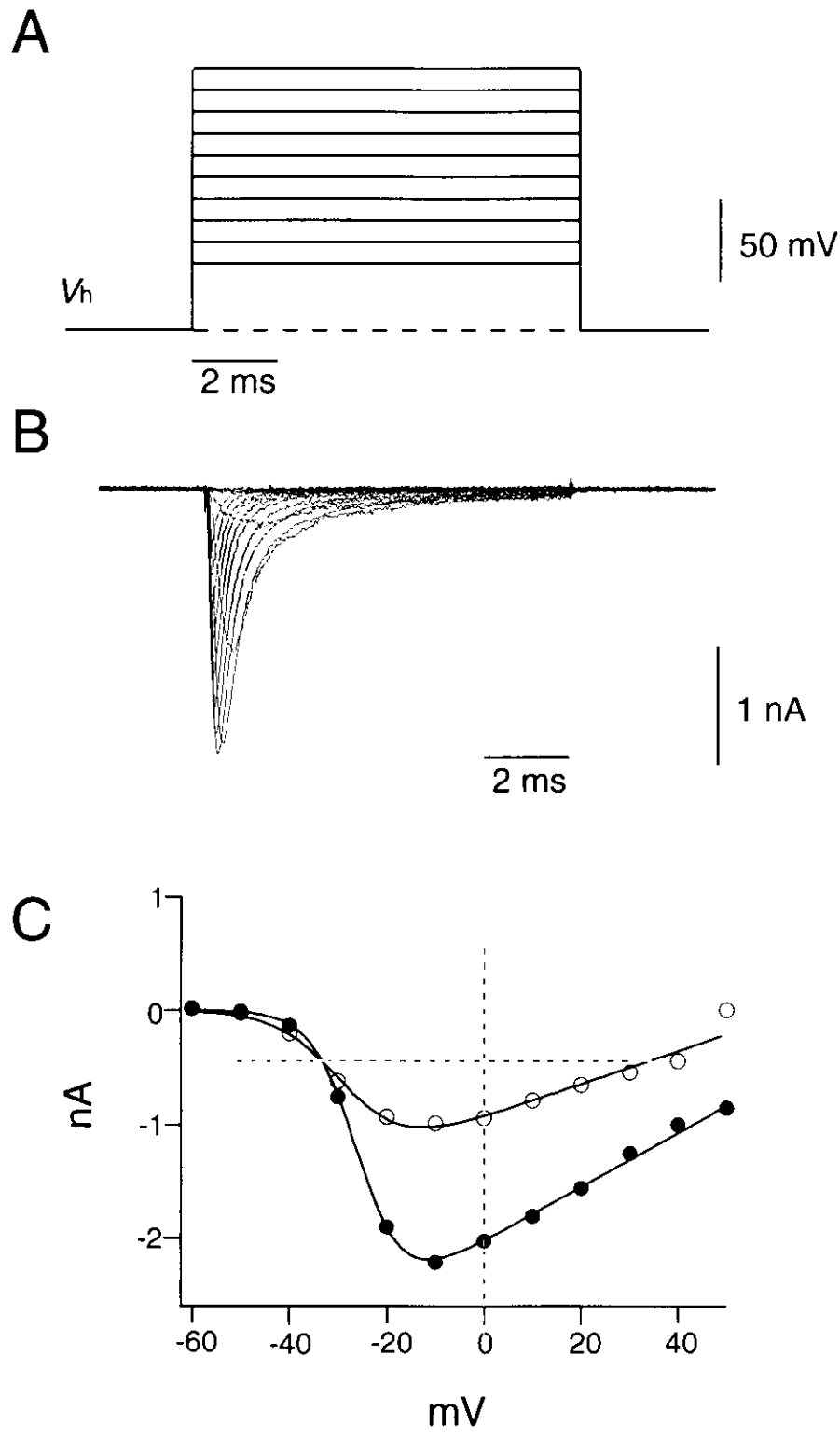

Figure 14

Figure 14: ***Whole-cell Na^+ current and I_{peak}-V relations.***

Current traces of WT (B) in response to depolarizing pulses (A). Holding potential (V_h) was –100 mV. The rectangular pulse potential was varied from –60 to +50 mV in 10 mV steps. The duration of each pulse was 10 ms. C, plots of peak currents *vs.* pulse potential (●, WT; ○, E4).

A

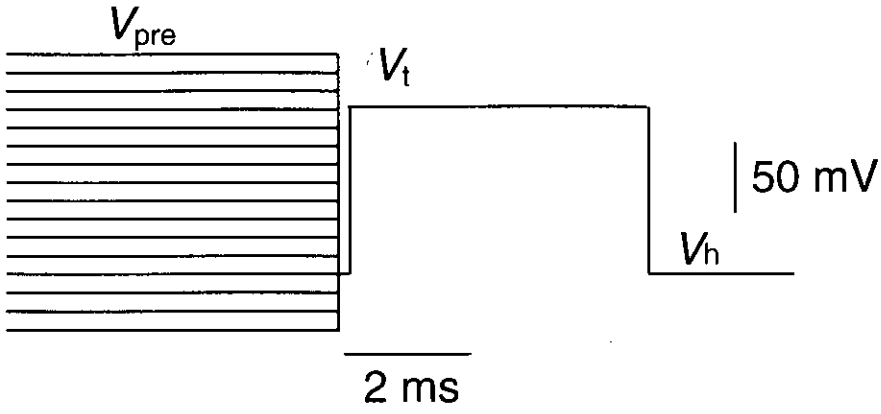

B

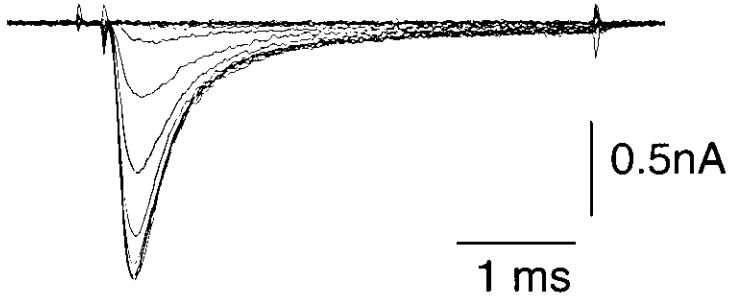

C

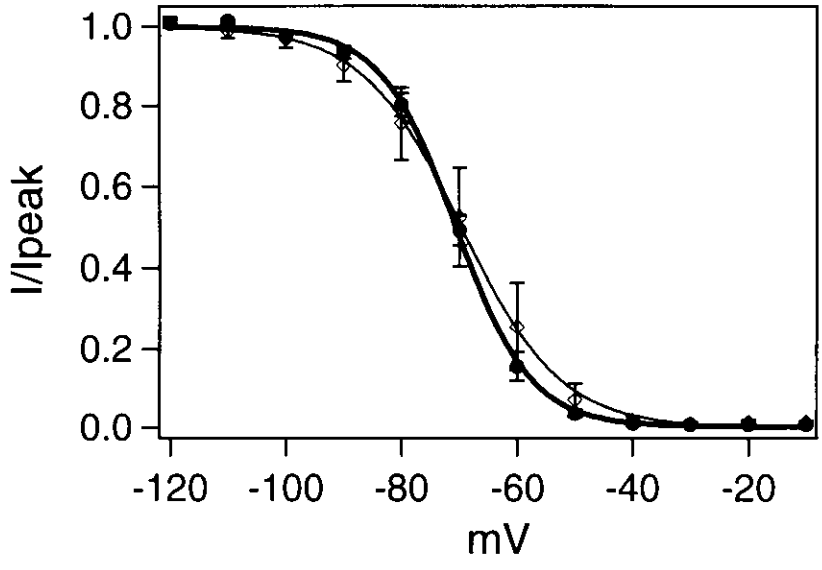

Figure 15

Figure 15; ***Voltage-dependence of inactivation.***

The upper set of traces shows the voltage protocol used to study the voltage-dependence of inactivation (A). A prepulse to V_{pre} of duration 200 ms was applied, immediately followed by V_h of 0.25 ms and a test pulse (V_t, -10 mV, 5 ms). V_{pre} was varied form –130 to 20 mV in 10 mV steps. The lower set of traces are WT currents (B). Panel C, peak currents at test pulses were normalized by their maximum value, observed when the prepulse was at –130 mV, and plotted against prepulse (●,WT; ○,E4). The data were fit with a two-state Boltzmann equation as described under Materials and Methods. Values represent averages, and error bars indicate S.E.M.

A

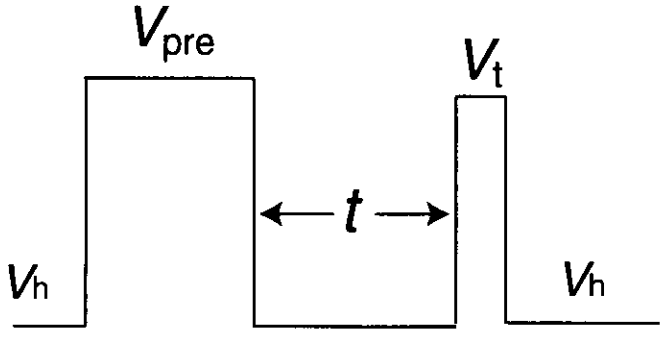
V_{pre}
V_t
t
V_h
V_h

B

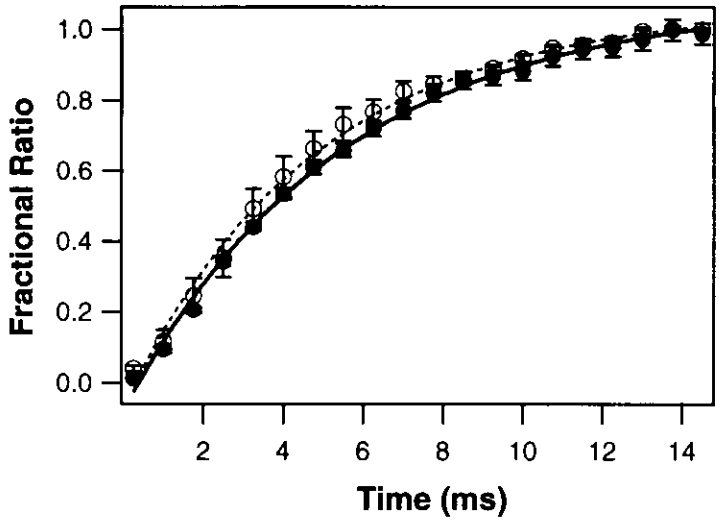
Fractional Ratio
1.0
0.8
0.6
0.4
0.2
0.0
2
4
6
8
10
12
14
Time (ms)

Figure 16

Figure 16; ***Recovery from inactivation.***

The time course of recovery of the channels from inactivation was studied using a voltage protocols (A). Channels were completely inactivated by a 200 ms depolarizing pulse, V_{pre}, to −10 mV and then held at V_h (-100 mV) for different durations followed by a step to the level V_t (-10 mV, 5 ms). Panel C. peak currents at a constant V_h but of different durations were measured, normalized by the steady-state value, and plotted against the time of recovery (●, WT; ○, E4). The time of recovery was varied from 0.5 to 14.75 ms by 0.75 ms steps. The continuous lines were fitted using single exponential equation, and error bars indicate S.E.M.

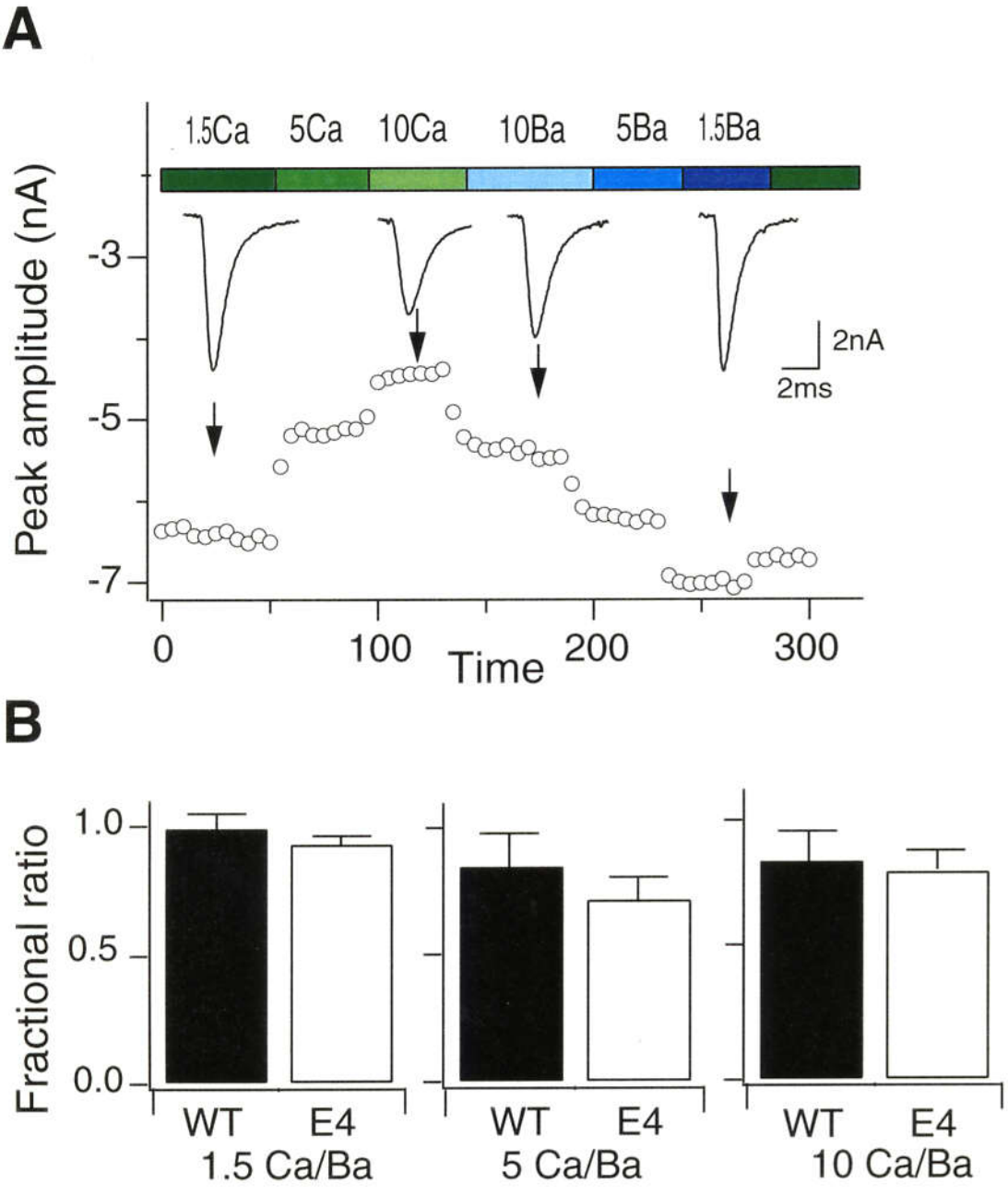
A
1.5Ca
5Ca
10Ca
10Ba
5Ba
1.5Ba
Peak amplitude (nA)
-3
-5
-7
2nA
2ms
0
100
200
300
Time
B
Fractional ratio
1.0
0.5
0.0
WT
E4
1.5 Ca/Ba
WT
E4
5 Ca/Ba
WT
E4
10 Ca/Ba

Figure 17

Figure 17; ***Divalent cationic effect (Ca^{2+} / Ba^{2+}) on the Na^{+} channel.***

(A) Extracellular divalent cations was exchanged from 1.5 mM to 10 mM Ca^{2+} (green in bar) and Ba^{2+} (blue in bar) in tyrode solution. Inward current was evoked every 5 seconds by a test pulse to 0 mV following a 200 ms prepulse to –80 mV, holding potential 100 mV. Current traces are at the indicated points. The bar graphs of SEM of the peak Ca2+/Ba2+ (1.5 mM, 5 mM and 10 mM divalent cations, n=4) show in (B).

Binding Scheme of NalQ and CaM

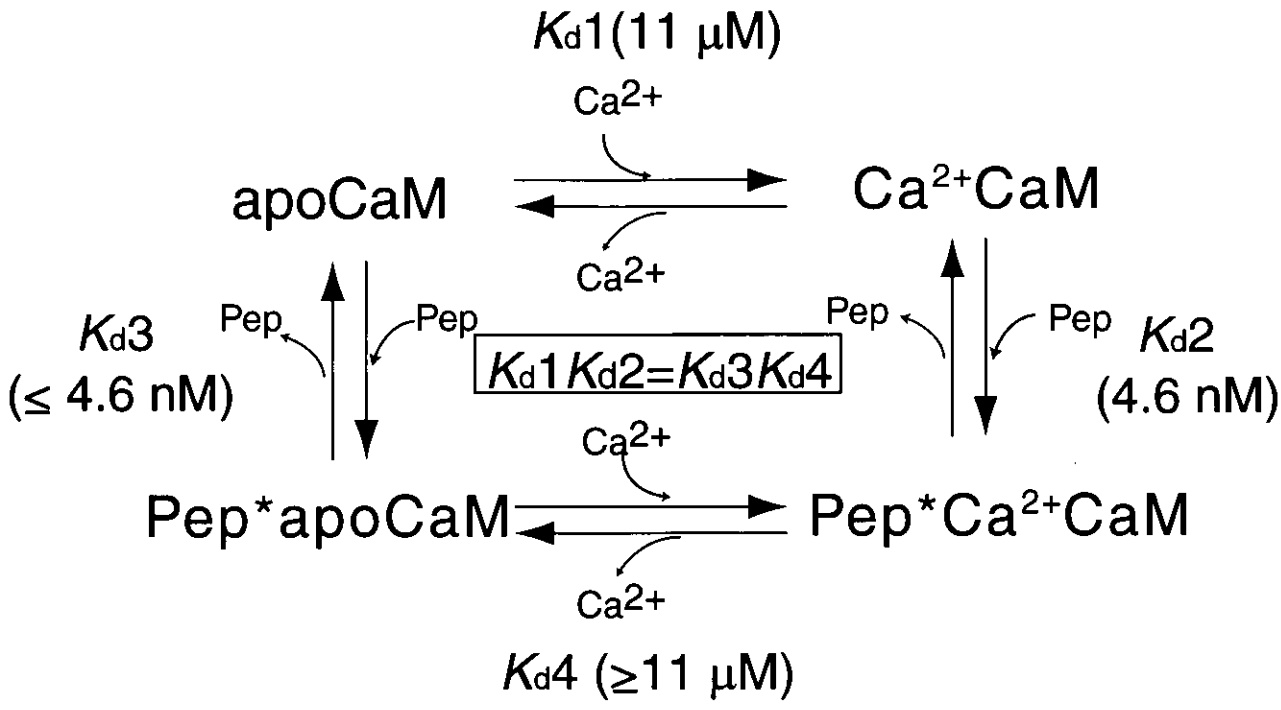

CaM; calmodulin, K_d; dissociation constant, Pep; NalQ peptide

Figure 18

Figure 18: ***Binding scheme of NaIQ and CaM.***

K_d2 and K_d4 value determined from the peptide titration (Figure 8) and from gel mobility shift assay compared with K_d2 (Figure 9), respectively. K_d1 value referred from ref 48. CaM; calmodulin, K_d; dissociation constant, Pep; NaIQ